FLOW FIELD IN A SKIMMING FLOW OVER A VERTICAL DROP WITHOUT END-SILL

Chang Lin * **S.-C. Hsieh**

Department of Civil Engineering
National Chung Hsing University
Taichung, Taiwan 40227, R.O.C.

W.-J. Lin

Fourth River Management Office
WRE, MOEA
Changhua, Taiwan 52441, R.O.C.

S.-H. Chou

Department of Civil Engineering
National Chung Hsing University
Taichung, Taiwan 40227, R.O.C.

R. V. Raikar

Department of Civil Engineering
K. L. E. S. College of Engineering and Technology
Belgaum 590008, India

ABSTRACT

The flow structure in the shear layer and in the recirculation zone of a skimming flow downstream of a vertical drop without end-sill measured using high speed particle image velocimetry (HSPIV) and flow visualization method is presented. The interface between the sliding jet and the recirculation zone (zone below sliding jet) was enhanced through non-ventilation condition between the drop structure and the jet. The flow field measured through HSPIV was used to represent the characteristics of mean streamwise velocity in the shear layer and mean horizontal velocity in the recirculation zone. With the growth of shear layer as the jet slides down over the recirculation zone, the momentum exchange from the sliding jet into the recirculation zone via the shear layer increases along with energy loss. Hence, it was observed that the amount of energy dissipated in the skimming flow at the drop structure without ventilation is greater than that with ventilation by an average value of 50% for $Y_c / H \geq 0.2$ (where Y_c = critical depth and H = drop height). However, the flow structure in the recirculation zone is found to be analogous to that of turbulent plane wall jet. The nonlinear regression analysis is used to fit the regressed velocity profiles to the measured HSPIV mean velocity distributions. Further, the appropriate characteristic velocity and length scales are selected to attain the unique similarity profiles both in the shear layer and in the recirculation zone of the skimming flow. The selection of the characteristic scales is also discussed. The similarity profiles are well comparable with those of napped flow without end-sill and with ventilation as well as of skimming flow with end-sill and without ventilation. It is interesting to observe that, the proposed similarity profiles for the shear layer also map the data of backward-facing step flow and cavity shear flow. In addition, the turbulence characteristics in the shear layer, including turbulence intensities, turbulent kinetic energy, viscous and Reynolds shear stresses, and turbulence energy-budget balance, are illustrated in detail. From the variation of turbulence production it is observed that near the drop structure the energy exchange is from the chaotic recirculation zone to the sliding-jet flow, while in the later part it is reversed. Furthermore, the analysis of turbulence energy-budget balance indicates very significant role of turbulence production, pressure diffusion and turbulence diffusion as compared with turbulence advection that has very minor role in turbulence energy-budget balance for the central part of the shear layer.

Keywords: Skimming flow, Shear layer, Turbulent energy budget, High speed particle image velocimeter, Similarity profile.

* Corresponding author (clin@mail.nchu.edu.tw)

DOI : 10.1017/jmech.2012.115
Copyright © 2012 The Society of Theoretical and Applied Mechanics, R.O.C.
https://doi.org/10.1017/jmech.2012.115 Published online by Cambridge University Press

1. INTRODUCTION

Drop structures constructed across the natural channel at regular intervals facilitate in tuning the slope of the channel bed in addition to their attribute as energy dissipators. Hence, they are frequently used in various hydraulic structures. In general, the drop structures are classified based on the downstream face as vertical drop and glacis type drop structure, and based on downstream floor condition: Drop with end-sill and drop without end-sill. In case of drop structures with end-sill, the energy dissipation occurs primarily due to mixing between the sliding jet and the downstream pool, which is supplemented by the cushion effect provided by the pool. On the other hand, for the drop structure without end-sill, no such cushion effect exists; hence, the energy loss is mainly attributable to turbulent mixings not only in the shear layer between sliding jet and recirculation zone but also inside the re-circulating zone (*i.e.*, the zone below sliding jet where the flow is of recirculation type).

Earlier studies on such drop structures mainly focused on the calculation of free surface elevation and estimation of relative energy loss of the dropping flow. The primary studies of the free overfall were serially presented by Rouse [1], White [2], Moore [3], and Rand [4]. Later, empirical equations of the relative energy loss of free overfall were reported by Rajaratnam and Chamani [5], Chamani and Beirami [6], Tokyay and Yildiz [7], and Lin *et al*. [8]. Chanson [9] and Huang [10] developed alternative empirical equations for predicting the impact position on channel bed due to the dropping flow downstream of a drop structure. Tokyay and Yildiz [7] also explored the relationship between the tail water depth and drop height by considering the effect of water depth right at the brink of a vertical drop. Recently, Chen *et al*. [11,12] investigated the impact force of dropping flow using an array of pressure transducers installed along channel bed and analyzed the distribution of pressure head on the channel bed downstream of a vertical drop.

Similar to the flow downstream of a vertical drop in the hydraulics, the flow downstream of a suddenly expanding duct or a cavity, which is usually termed as "backward (or rearward)-facing step flow" or "cavity shear flow" is significant in the traditional fluid-dynamics and aerodynamics researches. A bunch of papers can be found in the literature, *e.g.*, Etheridge and Kemp [13], Armaly *et al*. [14], Troutt *et al*. [15], Grant *et al*. [16], Pereira and Sousa [17], Kuo *et al*. [18] and Kuo and Jeng [19]. All of these works mainly focused on the velocity distributions or the coherent-structure dynamics in the separated shear flow, the mixing behavior in the recirculation bubble, the variation of reattachment length, the redeveloping turbulent boundary layer beyond separation-reattachment point, and so on. It is worth noting that, for all studies on the traditional backward-facing step flow and cavity shear flow, the separated flows were mainly driven by pressure force and the fluid was completely filled in the duct and cavity channel, in contrast to the characteristic of curving free surface of dropping flow, which is mainly subjected to gravitational force.

To the best knowledge of the authors, Rajaratnam and Chamani [5] was the first to initiate the measurement of velocity profiles of a dropping flow using Prandtl probes. Recently, the availability of advanced optical measuring techniques facilitated in visualizing and obtaining the flow domain at various structures. Lin *et al*. [8] used laser Doppler velocimeter (LDV) to investigate the characteristics of mean velocity fields in a falling jet, a sliding jet and the pool for a free overfall over a vertical drop without end-sill. The flow was napped with full ventilation. The characteristic velocity and length scales were proposed to develop similarity profiles of the mean velocity for falling and sliding jets and the pool. Later, Lin *et al*. [20] redefined the characteristic velocity and length scales for better similarity of the velocity profiles in the shear zone corresponding to the falling jet and the pool down the impingement line, following the proposal of Gaussian distribution for the similarity profiles for their data by Kiyani and Rajaratnam [21].

Furthermore, Lin *et al*. [22] identified three main types and two transitional types of flow patterns downstream of vertical drop particularly using flow visualization technique under subcritical approaching flow. They were a napped flow, a transitional flow between a napped flow and a periodic oscillating flow, a periodic oscillating flow, a transitional flow between a periodic oscillating flow and a skimming flow, and a skimming flow. This categorization depends upon the approaching flow discharge and geometry of drop structure such as drop height, pool length and end-sill height. In this study, the drop pool was created by an end-sill and it was non-ventilated. Recently, the mean velocity and turbulence characteristics in the shear layer of the skimming flow over a vertical drop under non-ventilation condition were presented by Lin *et al*. [23]. They used end-sills of different heights forming a pool on the downstream of the drop wall. Table 1 presents the list of the studies which mainly focus on the velocity field downstream of a vertical drop structure.

During high flood discharge, the effect of end-sill becomes insignificant, and the drop structure behaves as the one without end-sill. Also, due to larger flow depth corresponding to large discharge the aeration zone between the sliding jet and the pool is driven away resulting into the development of skimming flow without ventilation. In the aforementioned studies, the detailed investigation on the mean flow and turbulent structure in the skimming flow over a vertical drop without end-sill and without ventilation is lacking. Hence, the scope of the present study is to fill such gap and provide new data bank.

Therefore, the characteristics of the flow structure in the shear layer and in the recirculation zone of skimming flow over a vertical drop without end-sill and without ventilation are presented in the study. The flow visualization method was used to identify the skimming flow pattern. The mean streamwise velocity in the skimming flow and the mean horizontal velocity in the recirculation zone were measured using HSPIV. In order to create the skimming flow

https://doi.org/10.1017/jmech.2012.115 Published online by Cambridge University Press

Table 1 Review of studies on velocity field downstream of vertical drop structures

Authors	Drop structure	Flow pattern (s) studied	Measurement or analysis item (s) and tool (s)
Rajaratnam and Chamani [5]	A vertical drop (without end-sill)	Napped flow (with ventilation)	• Streamwise mean velocity profiles of sliding jet measured using Prandtl probe • Horizontal mean velocity profiles in recirculation zone using Prandtl probe
Lin *et al.* [8] Lin *et al.* [20]	A vertical drop (without end-sill)	Napped flow (with ventilation)	• Length of recirculation zone by flow visualization method • Streamwise mean velocity profiles measured by LDV • Horizontal mean velocity profiles in recirculation zone measured by LDV • Similarity profile for streamwise mean velocity in sliding jet
Lin *et al.* [22]	A vertical drop pool (with end-sill)	Napped flow, transitional flow, periodic oscillatory flow, transitional flow, skimming flow (all without ventilation)	• Classification of flow patterns by flow visualization method • Time histories of free surface elevation by wave gauge • Phase averaged velocity fields of both single phased water region and multi-phased aerated region of a periodic oscillatory flow by PIV and bubble image velocimeter (BIV) respectively.
Lin *et al.* [23]	A vertical drop pool (with end-sill)	Skimming flow (without ventilation)	• Identification of skimming flow pattern by flow visualization method. • Mean stream and normal velocity profiles in 2D shear layer region between sliding jet and pool by PIV. • Turbulence characteristics in shear layer region obtained by using PIV.
Present study (2011)	A vertical drop (without end-sill)	Skimming flow (without ventilation)	• Identification of skimming flow pattern by flow visualization method. • Mean stream velocity profiles in shear layer obtained by high speed PIV. • Vertical distributions of mean horizontal velocity in recirculation zone region by PIV • Turbulence characteristics in shear layer region obtained by using high speed PIV. • Turbulent energy balances in shear layer region analyzed using high speed PIV data.

condition, the ventilation was totally arrested. The effect of non-ventilation on the efficiency of drop structure in energy dissipation is studied. In addition, the important characteristic velocity and length scales are proposed for the similarities of velocity profiles both in the shear layer and in the recirculation zone. Furthermore, the turbulence characteristics in the shear layer along with turbulent energy budget balances are discussed.

2. EXPERIMENTAL SETUP AND CONDITIONS

An 8.85m long recirculation water flume located at the Hydraulics Laboratory of the Department of Civil Engineering, National Chung Hsing University, Taiwan was used to carry out the experiments. The test section was located at 3.0m from the flume inlet section having necessary arrangement to remove flow irregularities and attain flow uniformity. The details of the performance of the re-circulating water channel were described in Lin *et al*. [8]. The dimensions of the test section being 3.05m long, 0.5m wide and 0.54m deep consisted of glass-sided walls and glass bottom facilitating the optical observations through the entire flow domain.

Two 110cm long vertical drop models made of acrylic plates having drop height H = 11cm and 14cm were used in the experiments. The skimming flow condition was created at the vertical drop by providing necessary air tightness. The downstream of the vertical drop wall was kept free from any obstacles that could otherwise act as an end-sill. Figure 1(a) shows the schematic view of a vertical drop and the coordinate systems used. Two coordinate systems were used in the present study namely: Cartesian coordinate system and local coordinate system. The Cartesian coordinate system (X, Y) was considered with its origin located at the lower corner of the drop wall, while the local curvilinear coordinate system (S, Y_n) along the upper surface of the sliding jet having its origin immediately above the origin of Cartesian coordinate system as illustrated in Fig. 1(a). Here, S was measured tangentially along the upper surface of the jet and Y_n measured normal to the free surface of the jet with positive pointing outwards.

Total nine experiments (six experiments with 11 cm drop height and three experiments with 14cm drop height) were performed at varying approaching flow conditions having Y_c / H = 0.334 to 0.632. The various experimental parameters are furnished in Table 2. In Table 2 and in Fig. 1(a), q represents unit discharge, Y_a is the approaching flow depth, Y_c is the critical flow depth (= $\sqrt[3]{q^2/g}$), U_a is the approaching flow velocity, U_c is the critical velocity (= $(gY_c)^{1/2} = q / Y_c$), F_r is the approaching flow Froude number (= $U_a / \sqrt{gY_a}$), L is the length of recirculation zone, U_s is the mean streamwise velocity in the shear layer, U_p is mean horizontal velocity in the recirculation zone and Z is the transverse (spanwise) direction.

The HSPIV system was used to measure the velocity field in the shear layer and in the recirculation zone region of the vertical drop. It consisted of a continuous output laser emitting 5-W argon-ion laser beam of 1.5mm diameter, a high-resolution digital camera, light sheet optics system, and a controlling and processing computer. The laser beam emitted from the light source was reflected by a mirror and passed through a cylindrical rod to form 1.5mm thick light sheet, which was then redirected in to the flow region through the glass bottom along the center line of the flume [see Fig. 1(b)]. Aluminum powder, having a mean diameter of 10μm and a specific gravity of 2.7, was used as the seeding particle in PIV measurements. The settling velocity of the Aluminum particles (according to Stoke's law) is less than 0.01cm/s, which is much

https://doi.org/10.1017/jmech.2012.115 Published online by Cambridge University Press

Table 2 List of experimental conditions

Case	H (cm)	q (cm^2/s)	Y_a (cm)	$Y_c = \sqrt[3]{\frac{q^2}{g}}$ (cm)	U_a (cm/s)	U_c (cm/s)	Y_c / H	$F_r = \frac{U_a}{\sqrt{gY_a}}$
A	11	221.67	3.64	3.69	60.90	60.10	0.335	1.019
B	11	299.75	4.70	4.51	63.78	66.46	0.410	0.939
C	11	345.43	4.97	4.95	69.50	69.78	0.450	0.995
D	11	437.37	5.30	5.80	82.52	75.41	0.527	1.144
E	11	574.34	6.20	6.95	92.64	82.64	0.632	1.188
F	11	494.29	5.70	6.31	86.72	78.33	0.574	1.160
G	14	475.78	5.63	6.13	84.51	77.57	0.438	1.137
H	14	399.66	4.98	5.46	80.25	73.19	0.390	1.148
I	14	345.62	4.36	4.67	72.39	67.65	0.334	1.107

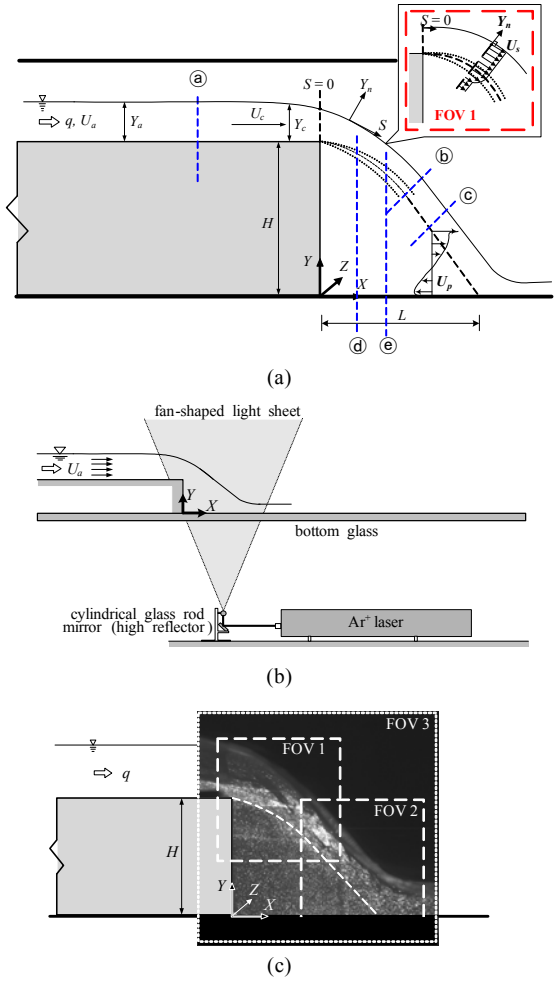


Fig. 1 (a) Schematic diagram of vertical drop structure and coordinate system; (b) Setup showing the field of view (FOV) of skimming flow region; and (c) Mean image of skimming flow for case $Y_c/H = 0.632$ (Case E)

smaller than any velocity of interest in this study. A high speed digital camera (Phantom from Vision Research) with 1024 × 1024 pixel resolution, 10-bit dynamic range, and 1,200Hz framing rate was used to capture the particle laden images. The camera mounted with 105mm focal lens was operated at 1,000 frames per second throughout the experiments. Velocity fields were determined by cross-correlation analysis using a multi-grid interrogation process starting at 32 × 32 pixels and ending with 8 × 8 pixels having 50% overlap. The images from three fields of views (FOVs) were taken using the HSPIV system [Fig. 1(c)] with the spatial resolution of about 0.95mm to 1.52mm. A sampling duration of 20.0s (*i.e.*, 20,000 images) was adopted for the HSPIV measurements.

For the validation of HSPIV measurements, the fiber-optic laser Doppler velocimeter (LDV) was used. The sampling duration of LDV measurements was 180s having sampling rate 100Hz. The velocity profiles measured by HSPIV at different sections as indicated (ⓐ ~ ⓔ) in Fig. 1(a) were compared with those measured by the LDV. In the present study, the maximum error between the measurements of mean velocity fields obtained by ensemble averaging 20,000 instantaneous velocity fields with HSPIV and LDV data at sections ⓐ, ⓑ, ⓒ, ⓓ and ⓔ were respectively 0.89%, 4.41%, 5.77%, 3.24% and 4.08% (not shown here). Similarly, the maximum error between the non-dimensional turbulence intensities $(\overline{u'u'})^{0.5}/U_c$ obtained by HSPIV and LDV measured at corresponding sections mentioned above were 0.35%, 1.23%, 2.06%, 5.47% and 1.02% respectively (not shown here). Further, the HSPIV measurement with a sampling duration of 20.0s (*i.e.*, 20,000 images) was considered as acceptable in the present study. This is because of two reasons: First the convergence of HSPIV measurements having 20,000 images with that of LDV measurements; and second because of sampling time (20.0 sec) is far larger than the integral time scale being equal to 0.099s.

3. RESULT AND DISCUSSIONS

3.1 Flow Pattern and Time-averaged Velocity Field in Skimming Flow

At first, the mean velocity profiles of approaching flow as well as corresponding flow right before and immediately after the brink of vertical drop are demonstrated in Figs. 2(a) ~ 2(f) for the experimental case $Y_c / H = 0.450$ (Case C). Note that, as shown in Fig. 1, the Cartesian coordinate (X, Y) and local curvilinear coordinate (S, Y_n) are used along with corresponding mean horizontal velocity U and mean streamwise velocity U_s in Figs. 2(a),2(b) and Figs. 2(c) ~ 2(f), respectively.

In Fig. 2(a), one can evidently observe the approaching flow with a relatively uniform distribution of the horizontal velocity $U(Y)$ measured at $X = -12.0$cm for $Y > 11.5$cm, except near the bed for 11.0cm < Y < 11.5cm where velocity gradient is prominent due to the boundary effect of upstream channel bed. For the flow right beyond the brink, say at $X = 0.0$cm and $Y >$ 11.0cm, the corresponding distribution of horizontal velocity can be witnessed in Fig. 2(b). It is found that the decrease in water depth (stemmed from the curving free surface which is subjected to gravitational force)

https://doi.org/10.1017/jmech.2012.115 Published online by Cambridge University Press

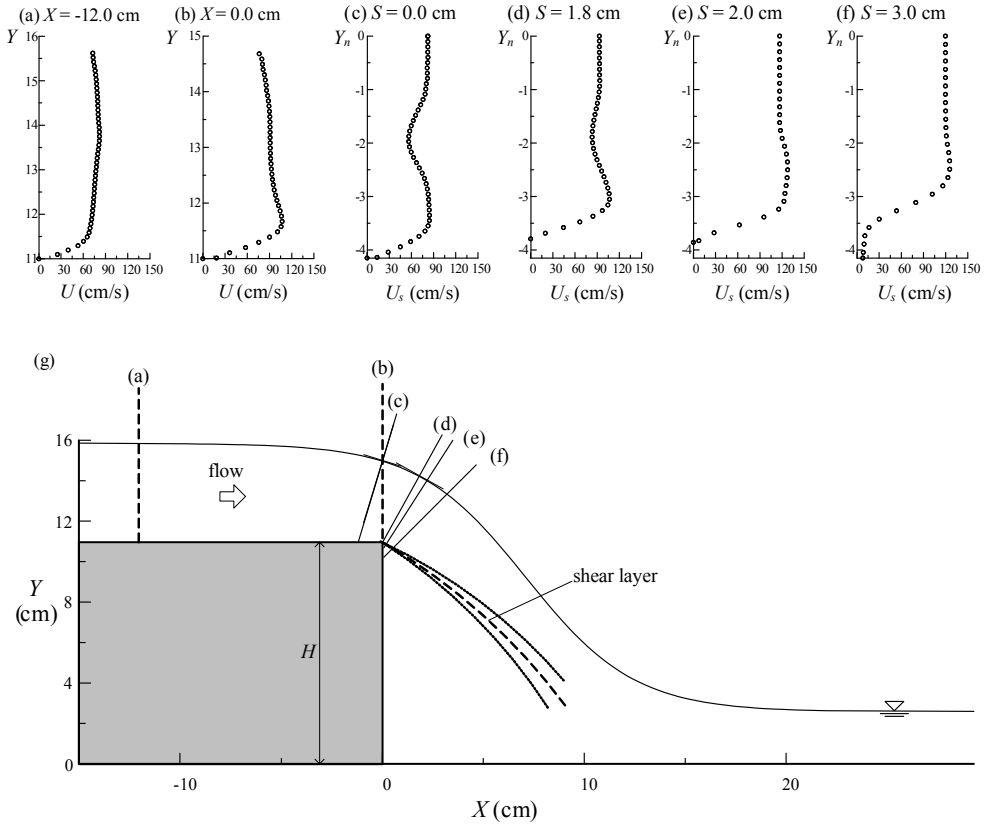


Fig. 2 Distributions of mean horizontal and streamwise velocities, $U(Y)$ and $U_s(Y_n)$ measured at (a) $X = -12.0$cm; (b) $X = 0.0$cm; (c) $S = 0.0$cm; (d) $S = 1.8$cm; (e) $S = 2.0$cm; and (f) $S = 3.0$cm for Case C

leads to the decrease in horizontal velocity near the water free surface. However, the *overshoot* in the horizontal velocity can be clearly evidenced at the lower portion located right beyond the boundary layer, as shown in Fig. 2(b). Such increase of horizontal velocity in the overshoot portion may be attributable to the constriction of water free surface (*i.e.*, the decrease in water depth over brink) and the constraint effect of upstream channel bed on the vertical velocity near the boundary. The magnitude of the overshoot of the streamwise velocity is 107.1cm/s.

On the other hand, for the flow right at the arc-length position of $S = 0.0$cm (*i.e.*, an inclined profile extending perpendicularly inwards from the curving free surface to a certain position situated on the upstream channel bed), a traditional velocity-deficit in the streamwise velocity profile $U_s(Y_n)$ can be seen clearly in Fig. 2(c) for the portion of $Y_n > -3.50$cm. For the remaining portion of $Y_n < -3.50$cm, the traditional boundary layer profile can be observed. Note that, at the free water surface right beyond the brink (*i.e.*, at $X = 0.0$cm and $S = 0.0$cm), the horizontal velocity U and streamwise velocity U_s are estimated to be 74.0cm/s and 82.2cm/s, respectively.

Furthermore, the streamwise velocity distribution $U_s(Y_n)$ right after drop measured at $S = 1.8$cm (*i.e.*, also an inclined profile extending perpendicularly inwards from the curving free surface exactly to the sharp corner of the brink) is depicted in Fig. 2(d). Both the velocity deficit in the central portion and the overshoot in the lower portion of streamwise velocity profile can be well identified. The maximum overshoot of the streamwise velocity is estimated to be 105.4cm/s, which is also the maximum velocity throughout the whole thickness of dropping flow. The streamwise velocity in Fig. 2(d) is in fact larger than that shown in Fig. 2(c) for the same Y_n value, except the position located in the lower portion for about $Y_n < -3.36$cm where the shear layer develops. It demonstrates the increase of streamwise velocity in the dropping flow right after the brink. For example, the streamwise velocity U_s being equal to 93.0cm/s just at the free surface of $S = 1.8$cm is actually larger than the counterpart of $S = 0.0$cm with $U_s = 82.2$cm/s.

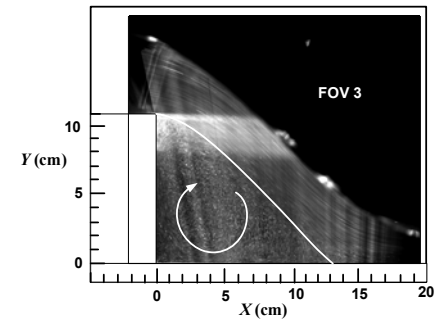
Figures 2(e),2(f) show the streamwise velocity profiles after the drop measured at the arc-length positions of $S = 2.0$cm and $S = 3.0$cm, respectively. It is important to mention that, for the same value of Y_n, nearly throughout the full thickness of dropping flow, the streamwise velocity measured at $S = 2.0$cm [Fig. 2(e)] is more than that at $S = 1.8$cm [see Fig. 2(d)]. However, the difference between the overshoot in the lower portion and the maximum deficit in the middle portion at $S = 2.0$cm become smaller as compared with that at $S = 1.8$cm. The flow becomes more uniform with continuous modification as seen from the streamwise velocity of dropping flow in Fig. 2(f). It is pertinent to observe that the streamwise velocity distribution becomes fairly uniform in the upper and middle portions for $Y > -2.7$cm, although slight overshoot can be observed for $-2.7\text{cm} < Y < -2.0$cm. On the other hand, very prominent streamwise velocity gradient exists in

https://doi.org/10.1017/jmech.2012.115 Published online by Cambridge University Press

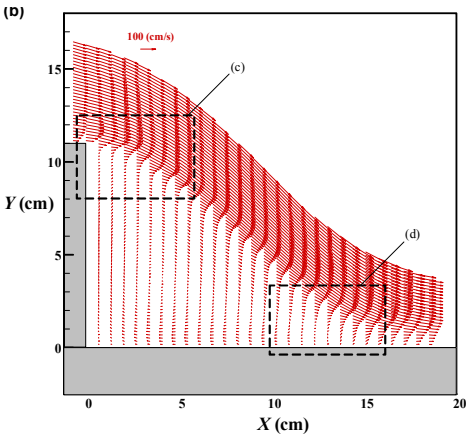
the lower portion of the dropping flow for $Y < -2.7$cm, demonstrating the development of a shear layer beneath the dropping flow (*i.e.*, the sliding jet).

It is worth noting that the streamwise velocity U_s on the free surface of dropping flow at $S = 0.0$, 1.8, 2.0, and 3.0cm shown in Figs. 2(b) ~ 2(f) for Case C are estimated to be 82.2, 93.0, 116.7 and 119.6cm/s, respectively, indicating the increase of the free-surface streamwise velocity right after the drop as a result of gravity. Due to the existence of brink at the top of a vertical drop, the velocity distributions measured right before and after dropping shown in Figs. 2(b) ~ 2(f) also depict the successively abrupt changes of streamwise velocity and the re-distribution process of velocity profiles.

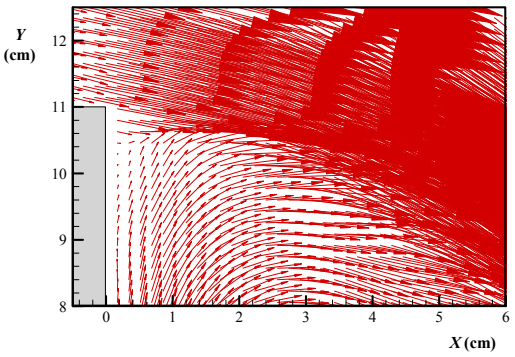
The typical flow pattern of a skimming flow for the experimental case $Y_c / H = 0.632$ (Case E) and the corresponding time-averaged (mean) velocity field are presented in Figs. 3(a) and 3(b) respectively. The sliding of the overlaying surface jet over the recirculation zone can be distinctly observed from Fig. 3(a). The mean streamwise velocity of the sliding jet increases in the downstream direction as illustrated by the time-averaged velocity field in Fig. 3(b). This is due to the gravity effect of the drop structure. In addition, it is also interesting to see a larger sized clockwise vortex occupying the entire recirculation zone. The vortex becomes stronger due to the momentum exchange of the shear layer between sliding jet and recirculation zone as well as from the deflected flow the drop wall. Figures 3(c), 3(d) show the close-up views of recirculation zone near the drop wall and close to the base of the drop structure, respectively. From Figs. 3(c),3(d) it is evident that the size of the recirculation zone is very large, which enhance in the energy loss. Also, the skimming flow of sliding jet over recirculation zone can be witnessed. The position of bifurcation of the sliding jet at the bottom of the floor into the recirculation zone is also illustrated in Fig. 3(d) with enlarged view, which defines the length of recirculation zone, L. It is important to note that, the determination of the length of recirculation zone L is very essential to study the mean flow characteristics in the recirculation zone. However, in case of falling jet of napped type, the flow in the recirculation zone region is circulating along with chaotic turbulence as reported by Lin *et al*. [8]. Lin *et al*. [8] also observed that the vortex occurs near the sliding jet, while circulations near the drop wall were rather random in nature. In the present case of skimming flow, the vortex, which is stronger and more prominent, is responsible for the momentum exchange between the sliding jet and the recirculation zone. This can also be substantiated from the velocity field shown in Fig. 3(b). Further, from Fig. 3(b), one can observe the existence of very large velocity gradient between the sliding jet and the recirculation zone forming a shear layer facilitating in larger energy and momentum exchange. This causes the decrease in the velocity gradient and increase in the thickness of the shear layer in the streamwise direction. Similar observations were also reported for the case of napped flow between falling and sliding jet by Lin *et al*. [8] and for the skimming flow at the vertical drop pool with end-sill by Lin *et al*. [23].



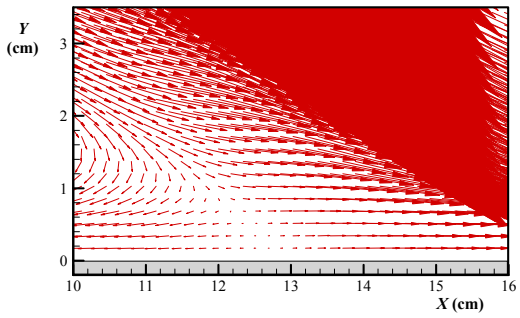
(a)



(b)



(c)



(d)

Fig. 3 Flow patterns of skimming flow: (a) Mean image of skimming flow obtained by HSPIV; (b) Corresponding mean velocity field; (c) Close-up view of mean velocity field near brink of vertical drop; and (d) Enlarged view of mean velocity field near base of vertical drop for $Y_c/H = 0.632$ (Case E)

https://doi.org/10.1017/jmech.2012.115 Published online by Cambridge University Press

3.2 Energy Loss at Vertical Drop

The energy loss at vertical drop structures has been studied extensively for decades as it is one of the prime functions of a drop structure. Rajaratnam and Chamani [17] investigated the variation of relative energy loss $\Delta E/E_1$ with Y_c / H at a drop structure combining the data of Moore [3] and Rand [4]. They expressed the relative energy loss in terms of Y_c / H as:

$$\frac{\Delta E}{E_1} = 0.0896\left(\frac{Y_c}{H}\right)^{-0.766} \tag{1}$$

where $\Delta E = E_1 - E_2$; E_1 = energy at upstream of drop structure; and E_2 = energy at downstream of drop structure (Rajaratnam and Chamani, [5]). They also indicated that most of the energy loss occurs due to the mixing between the sliding jet and the recirculation zone. However, the study of Rajaratnam and Chamani [5] was with ventilated drop structure. The results of Lin *et al.* [8] on energy loss using LDV fitted well with Eq. (1). Jaung [24] investigated the effect of non-ventilation on the relative energy loss of a vertical drop. The results indicated that the relative energy loss without ventilation effect is higher than that with ventilation effect. The data points obtained in the present study also follows the trend of Jaung [24]. Nevertheless, the present study emphasizes the skimming flow condition without the ventilation at drop structure. The variation of the relative energy loss $\Delta E/E_1$ with Y_c / H is plotted in Fig. 4 and the data points collapse onto a single band with a regression curve expressed as ($R^2 = 0.896$):

$$\frac{\Delta E}{E_1} = 0.181\left(\frac{Y_c}{H}\right)^{-0.442} \tag{2}$$

In Fig. 4, it is promising to observe that the value of relative energy loss for non-ventilated skimming flow is larger than that for the ventilated dropping flow. The trend line for non-ventilation condition deviates at $Y_c / H = 0.12$. However, the increase in relative energy loss $\Delta E/E_1$ obtained by Eqs. (1) and (2) is about 50% (average value) for the value of $Y_c / H \geq 0.2$. The maximized length of interface between sliding jet and recirculation zone for non-ventilation condition in skimming flow is the reason for greater efficiency in relative energy loss, which corroborate with Rajaratnam and Chamani [5]. However, for $Y_c / H < 0.2$, the variation of the relative energy loss approaches that of the ventilation case.

4. MEAN VELOCITY PROFILES IN SHEAR LAYER BETWEEN SLIDING JET AND RECIRCULATION ZONE

The instantaneous velocities measured by the HSPIV are ensemble averaged to obtain the mean velocity $U_s(Y_n)$ along the streamwise direction of the sliding jet of the skimming flow. Figure 5 represents the profiles of the mean streamwise velocity $U_s(Y_n)$ in the shear layer structure between the sliding jet and the recirculation zone for Y_c / H = 0.335, 0.410, 0.450, 0.527, and 0.632 (Cases A-E) at different cross-sections having respective arc-length position S (with $S = 0$ at the brink of the drop). It is interesting to observe from Fig. 5(a) that the velocity gradient within the shear layer near the drop (*i.e.*, at S = 2.0 ~ 4.0cm) is very large and decreases as the jet slides downstream over the recirculation zone. This is similar to the results reported by Lin *et al.* [8] for the napped flow without end-sill and with ventilation and Lin *et al.* [23] for the skimming flow with end-sill and without ventilation. It substantiates the phenomenon of momentum exchange and turbulent mixing between the sliding jet and recirculation zone and hence responsible for the increase in thickness of shear layer. From the close observation of Figs. 5(a) and 5(b), it can also be visualized that the position of the shear layer shifts downwards as Y_c / H increases, which is due to the gravitational effect on the falling jet. However, beyond the shear layer, the mean streamwise velocity $U_s(Y_n)$ remains almost constant both in the recirculation zone and in the sliding jet.

Further, the analysis proposed by Lin *et al.* [20] is particularly used to determine the velocity and length scales for obtaining the similarity profile of the mean streamwise velocity $U_s(Y_n)$ by using the measured data at different cross-sections. Here, the method of nonlinear curve fitting to the experimental data was implemented. The equation for the mean streamwise velocity $U_s(Y_n)$ is expressed as

$$U_s(Y_n) = C_1 \tanh(C_2\, Y_n + C_3) + C_4 \tag{3}$$

where C_1 to C_4 are regression coefficients (available in Chou, [25]). The fitting curves are shown in red color in Fig. 5, which demonstrates the satisfactory fitting of curves to the experimental data. This implies that the representative velocity and length scales can be derived precisely from these curves.

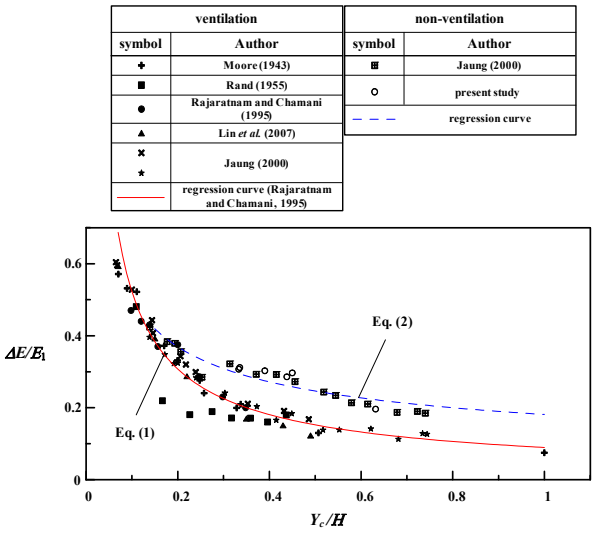


Fig. 4 Variation of the relative energy loss $\Delta E/E_1$ with Y_c/H

https://doi.org/10.1017/jmech.2012.115 Published online by Cambridge University Press

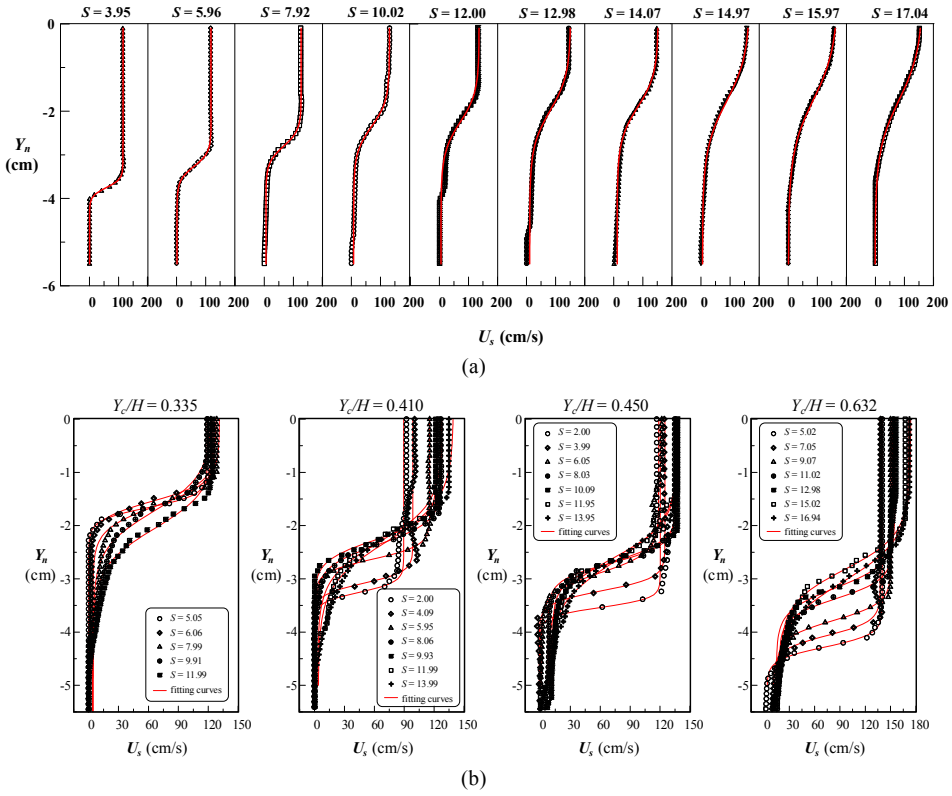


Fig. 5 Mean streamwise velocity profiles in shear region between sliding jet and recirculation zone along with fitting curves for Y_c/H =: (a) 0.527 (Case D); (b) 0.335, 0.410, 0.450 and 0.632 (Cases A, B, C, E)

The similarity profile for the mean streamwise velocity $U_s(Y_n)$ within the shear layer was obtained using the method proposed by Lin *et al.* [20]. Figure 6 illustrates different curves used for the purpose, for the experimental case $Y_c / H = 0.527$ (Case D) at the arc-length position of $S = 5.00$cm. The variation of mean streamwise velocity $U_s(Y_n)$, its first derivative $\partial U_s / \partial Y_n$ (representing the viscous shear stress) and second derivative $\partial^2 U_s / \partial Y_n^2$ (denoting the slope of viscous shear stress) with respect to the distance Y_n normal to the upper surface of the jet are plotted in Fig. 6. It is pertinent to mention that the first and second derivatives were calculated directly using the $U_s(Y_n)$ fitting curves of Eq. (3), without using interpolation or extrapolation to the data points. The center position of the shear layer is located at the occurrence of maximum value of $\partial U_s / \partial Y_n$ and is expressed as Y_{nc} (Fig. 6). Further, Y_{nu} and Y_{nd} represent respectively the upper and lower bounds of the shear layer which were defined at respective points where the extrema of $\partial^2 U_s / \partial Y_n^2$ occur, as shown in Fig. 6. Here, U_u and U_d represent the mean velocities at respective points Y_{nu} and Y_{nd}. Using these, the specific velocity scale, $(U_u - U_d)$ and the corresponding specific length scale, $b_s = (Y_{nu} - Y_{nd})$, are defined to formulate the similarity velocity profile. To be precise, b_s denotes the *representative thickness* of the shear layer while $(U_u - U_d)$ represents the velocity deficit between the upper and lower bounds of the shear layer defined in b_s.

Besides, another length scale, b_s^* representing the practical thickness of shear layer is considered for its suitability in obtaining the similarity profile. The

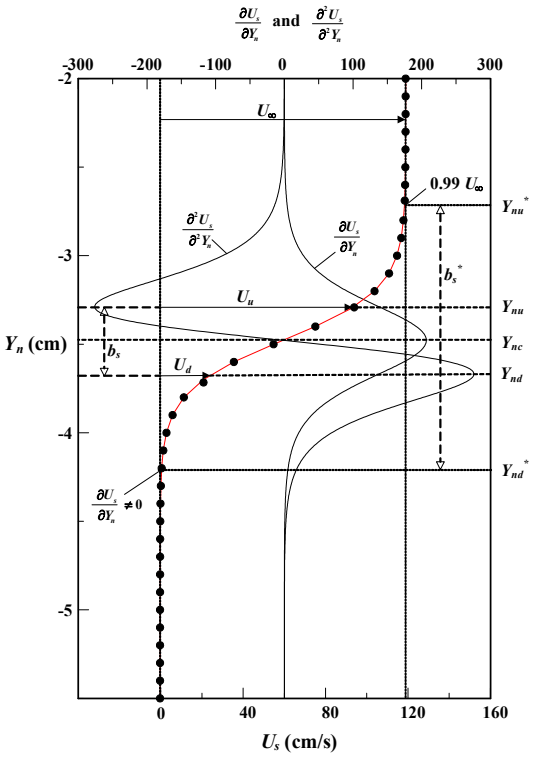


Fig. 6 Variation of U_s, $\partial U_s / \partial Y_n$, and $\partial^2 U_s / \partial Y_n^2$ with Y_n for $Y_c / H = 0.527$ (Case D) at $S = 5.00$cm

https://doi.org/10.1017/jmech.2012.115 Published online by Cambridge University Press

length scale, $b_s^* = (Y_{nu}^* - Y_{nd}^*)$, where Y_{nu}^* represent the upper bound location corresponding to the mean streamwise velocity $U_s = 0.99U_\infty$, U_∞ is the mean streamwise velocity beyond shear layer, and Y_{nd}^* represent the lower bound location at which the velocity gradient of mean streamwise velocity is $\partial U_s / \partial Y_n \neq 0$ (see Fig. 6). Figure 7(a) showing the variation between b_s and b_s^* for Y_c / H = 0.335, 0.450, and 0.632 (Cases A, B, E) indicate the linear relationship between b_s and b_s^* having marginal difference in slope. Hence, the combined relationship expressed as Eq. (4) is obtained between b_s and b_s^* with the R^2 value of at least 0.98 as plotted in Fig. 7(b).

$$b_s^* = 5.15 \times b_s \tag{4}$$

This indicates that any one of the two length scales amongst b_s and b_s^* could be selected for obtaining the similarity profile. In addition, Eq. (4) represents that the representative thickness of the shear layer b_s is 0.194 times the practical thickness of shear layer b_s^* (*i.e.*, $b_s = 0.194 \times b_s^*$). However, Lin *et al.* [23] obtained representative thickness of the shear layer b_s as 0.2 times the practical thickness of shear layer b_s^* for the case of skimming flow at the vertical drop with end-sill and without ventilation ($b_s = 0.200 \times b_s^*$). The existence of end-sill would be probably responsible for slight higher value of representative thickness of the shear layer b_s. Based on the observation and analysis, authors anticipated that $(U_u - U_d)$ and b_s (representative thickness) could be the appropriate characteristic velocity and length scales for developing the similarity profile between mean streamwise velocity U_s and Y_n. Consequently, the variation of the dimensionless mean velocity deficit $(U_s - U_d)/(U_u - U_d)$ versus the dimensionless shear layer thickness $(Y_n - Y_{nc})/b_s$ is plotted in Fig. 8. It is interesting to observe that the data of all experimental series collapse on a single band with a similarity profile expressed by Eq. (5) having a R^2 value of 0.996.

$$\frac{(U_s - U_d)}{(U_u - U_d)} = 0.833 \tanh\left[1.450\left(\frac{Y_n - Y_{nc}}{b_s}\right) + 0.050\right] + 0.525 \tag{5}$$

It is important to mention that this similarity equation is valid for $3.0 < S < 17.5$ throughout all the experimental cases. The velocity profiles shown in Figs. 2(b) ~2(f) for the sections right before, exactly at, and immediately after drop (*i.e.*, $S < 3.0$cm) are not considered. This is because these velocity profiles successively experience abrupt changes and re-distribution process and hence do not have the appropriate length and velocity scales to constitute the similarity profile.

The result illustrated by Eq. (5) shows a promising similarity profile corresponding to the shear layer structure between the sliding jet and the recirculation zone for different Y_c / H ratios and different cross-sections from the vertical drop. Figure 9 presents the comparison of similarity profiles for the mean streamwise velocity U_s obtained in the present study

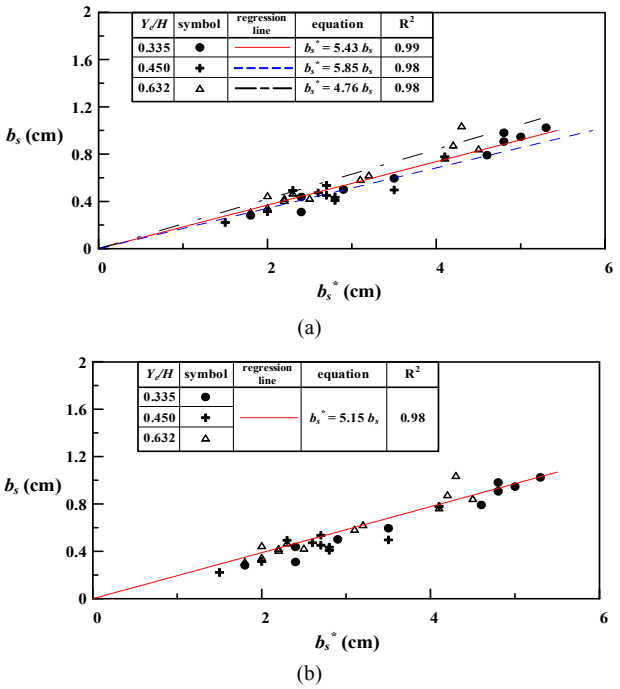


Fig. 7 Variation of b_s and b_s^* for Y_c / H = 0.335, 0.450, and 0.632 (Cases A, B, E): (a) with separate regression line for each case; (b) with common regression line of all three cases

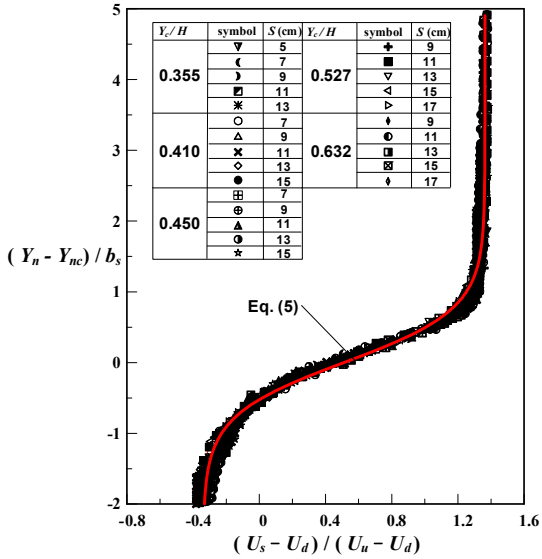


Fig. 8 Similarity profile for mean streamwise velocity in shear layer between sliding jet and recirculation zone

(skimming flow over vertical drop without end-sill and without ventilation) with those of skimming flow over vertical drop with end-sill and without ventilation [Lin *et al.* [23]] and of napped flow without end-sill and with ventilation [Lin *et al.* [20]]. All three similarity profiles follow the same trend. Further, all three similarity curves overlap in the upper part of the shear layer, while in the lower portion they deviate slightly. This is attributable to the effect of ventilation and end-sill.

https://doi.org/10.1017/jmech.2012.115 Published online by Cambridge University Press

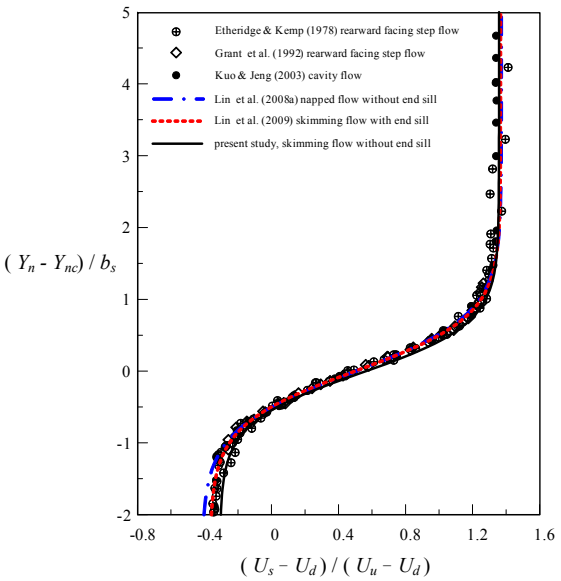


Fig. 9 Comparison of similarity profiles for mean streamwise velocity in shear layer of skimming flow and napped flow with and without end-sill, along with experimental data points from previous investigations on traditional rearward-facing step flow and cavity shear flow

Moreover, the experimental data points from the studies of traditional backward-facing step flow (Etheridge and Kemp, [13]; Grant *et al*., [16]) and cavity shear flow (Kuo and Jeng, [19]) are also included in Fig. 9., showing the overall trend of data points measured in different separated shear layers is in good agreement with these three similarity curves. It should be emphasized that, for the studies on traditional backward-facing step flow and cavity shear flow mentioned above, the separated flows were driven by pressure force and without the free surface effect, thus leading to the domination of Reynolds number on the flow. However, for the present case of skimming (and even for napped) flow downstream of a vertical drop, the flows are mainly driven by gravity force associated with prominent water free-surface effect, thereby resulting the dropping flow with very curving free surface so called the falling and sliding jets. In the present cases, the most important parameter is Froude number. Although the forcing mechanism of dropping flow is very different from that of the traditional backward-facing step flow and cavity shear flow, the similarity profile of the streamwise velocity obtained herein is still valid for the traditional backward-facing step flow and cavity shear flow. This strongly demonstrates the effectiveness of proposed method to determine the characteristic length and velocity scales by Lin *et al*. [8] and by this study for generalized shear flow cases.

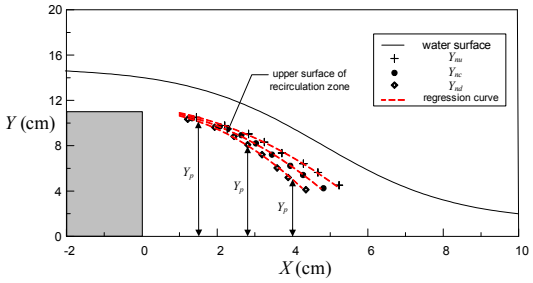
5. MEAN VELOCITY PROFILES IN RECIRCULATION ZONE

The skimming jet leaving the vertical drop slides continuously over the recirculation zone and impinges on the floor. The majority of its flow goes downstream while a small quantity enters the recirculation zone. In the interface between the shear layer and recirculation zone the energy and momentum gets transferred to the recirculation zone thereby resulting into energy dissipation. This re-circulating flow is primarily responsible for the momentum transfer and energy dissipation. The depth of recirculation zone defined by the upper surface Y_p was determined from the lower bound of the shear layer Y_{nd} of the sliding jet (see Fig. 6). Figure 10(a) illustrates the thickness of shear layer defining the profiles of the centerline Y_{nc}, upper bound Y_{nu} and lower bound Y_{nd} for $Y_c / H = 0.335$ (Case A). These profiles are obtained from the regression curves fitted to the mean streamwise velocity profiles of sliding jet having the R^2 value of 0.996. Similar procedure was adopted for other experimental cases.

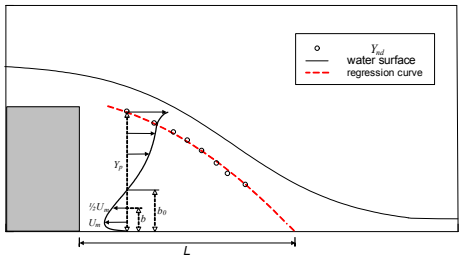
The mean horizontal velocity U_p in the recirculation zone was obtained by ensemble averaging of the instantaneous velocities measured by the HSPIV for different experimental cases. Figure 11 represents the vertical distributions of the mean horizontal velocity U_p for the experimental case $Y_c / H = 0.632$ (Case E) measured at various X/L ranging from 0.092 to 0.957, where X is the distance from the drop wall. It is interesting to note that the profile of the mean horizontal velocity U_p follow a particular trend at all X/L values. The value of mean velocity U_p increases with negative value from zero at bottom of the recirculation zone reaching a negative maximum value U_m ($U_m < 0$) and then decreases to become positive and increases towards the top of the recirculation zone. The value of U_p reaches negative maximum value U_m at vertical distance Y from the bottom of the recirculation zone nearly in the range of 0.1cm to 0.5cm. Then U_p decreases to zero approximately at Y = 1cm to 4cm, above which U_p increases in the positive direction. The magnitude of $-U_m$ increases with an increase in distance X from the drop wall and its location becomes closer to the base of the recirculation zone with increase in X. However, above the recirculation zone the nature of variation of U_p changes abruptly. This is due to influence of the sliding jet of the shear layer. Hence, the demarcation line of the recirculation zone is marked as the lower bound Y_{nd} of the shear layer. From the mean horizontal velocity profiles of U_p, it is interesting to observe that the flow gets deflected near the base of the recirculation zone stemming from the bifurcation of the sliding jet and moving towards the vertical drop wall. Therefore, by observation of vertical distribution of mean horizontal velocity U_p in the recirculation zone, the definition sketch as illustrated in Fig. 10(b) is drawn following Lin *et al*. [8], in which U_m denotes the negative maximum value of U_p, b represents the value of Y at $U_p = U_m / 2$, and b_0 represents the value of Y at $U_p = 0$ (the edge of the deflected jet). The values of $-U_m$, b and b_0 are determined from all mean velocity profiles of U_p for each of experimental cases.

Figures 12(a) and 12(b) show the variation of dimensionless values of b_0 / Y_p and b/Y_p with dimensionless recirculation zone length X/L for experimental cases of Y_c / H = 0.335 (Case A), 0.450 (Case C) and

https://doi.org/10.1017/jmech.2012.115 Published online by Cambridge University Press



(a)



(b)

Fig. 10 Schematic diagram (a) Thickness of shear layer and upper surface of recirculating zone for $Y_c/H = 0.335$ (Case A); and (b) Velocity profile in recirculating zone defining various parameters

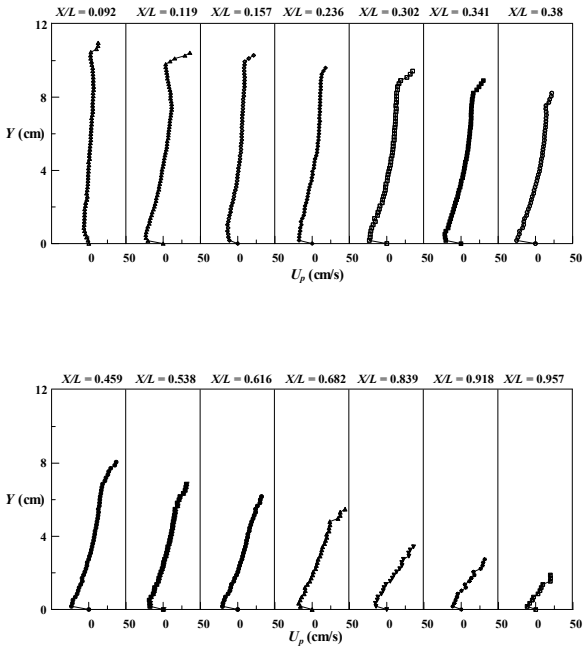
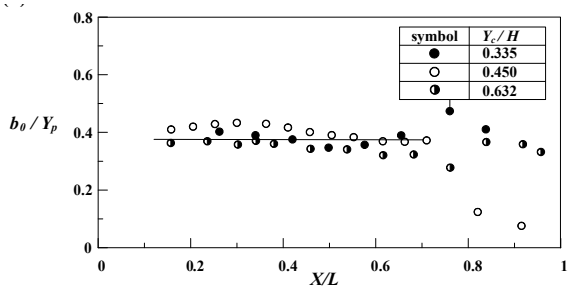


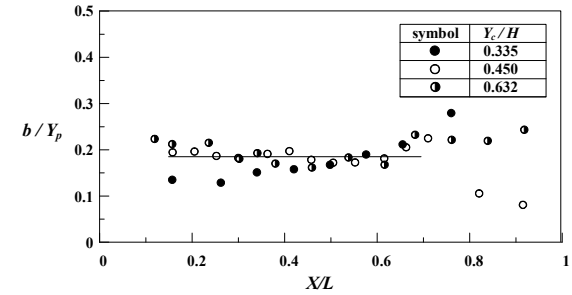
Fig. 11 Vertical distributions of mean horizontal velocity measured in the recirculating zone for $Y_c/H = 0.632$ (Case E) at different X/L values

0.632 (Case E). It is interesting to observe that the data plots fall along a linear band for $0.2 \le X/L \le 0.7$ with mean values b_0 / Y_p and b/Y_p being respectively 0.4 and 0.2. However, a greater scatter of the plots of b_0 / Y_p and b/Y_p is observed for $X/L \ge 0.7$. This is due to the smaller thickness of the recirculation zone at the end and deflection of the sliding jet creating more fluctuations.

Figures 13(a) and 13(b) show the variation of $-U_m$ with X and $(L - X)$, respectively for $Y_c / H = 0.335$



(a)



(b)

Fig. 12 Variations of (a) b_0 / Y_p, and (b) b/Y_p with X/L for $Y_c/H = 0.335$ (Case A), 0.450 (Case C), and 0.632 (Case E), respectively

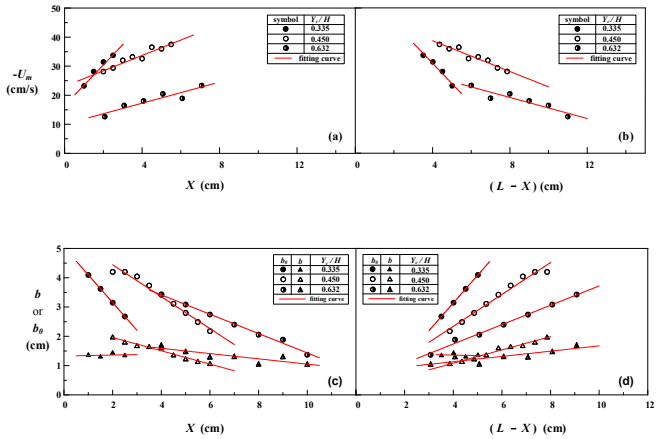


Fig. 13 Variations of (a) $-U_m$ with X; (b) $-U_m$ with $(L - X)$; (c) Y with X; and (d) b with $(L - X)$ for $Y_c / H = 0.335$ (Case A), 0.450 (Case C), and 0.632 (Case E), respectively

(Case A), 0.450 (Case C) and 0.632 (Case E). It can be observed that $-U_m$ increases linearly with an increase in distance X from the drop wall. This is due to the larger fluid momentum near the end of the recirculation zone, which decreases as the deflected jet moves towards the drop wall. It further substantiates the transfer of the energy from the sliding jet to the recirculation zone. The similar results were also reported by Lin *et al.* [8] for the case of falling and sliding jet (napped flow). On the other hand, $-U_m$ decreases with an increase in $(L - X)$. In addition, it is also observed that the slope of the variation of $-U_m$ is steeper for smaller value of $Y_c / H = 0.335$ (Case A) and getting flatter for larger value of $Y_c / H = 0.632$ (Case E).

Similarly, the variations of two length scales b and b_0

https://doi.org/10.1017/jmech.2012.115 Published online by Cambridge University Press

with respect to X and $(L - X)$, respectively, are furnished in Figs. 13(c) and 13(d). From Fig. 13(c), it can be seen that both b and b_0 decreases linearly with the increase in distance X. However, the decreasing rate is greater for b_0 than for b, signifying that the thickness of the deflected jet b_0 (that is the location of $U_p = 0$) reduces with an increase in value of X faster than b (that is half velocity depth at $U_p = U_m / 2$). This illustrates that the deflected jet from the sliding jet of skimming flow gets bifurcated into the recirculation zone thereby resulting in to recirculation and transfer of energy. On the contrary, the length scales b and b_0 increase with increase in $(L - X)$ as depicted in Fig. 13(d). It is important to note that the above discussion is for the case of skimming flow without ventilation and without end-sill. However, Lin *et al*. [8] illustrated similar phenomena along with the results for the case of napped flow with ventilation and without end-sill.

Based on the discussions mentioned above and using the characteristic dimensions of the mean horizontal velocity profile U_p, the similarity profiles are drawn for the mean horizontal velocity profiles in the recirculation zone following Lin *et al*. [8]. However, the data considered in obtaining the similarity profiles are for the cases $Y_c / H = 0.335$ (Case A), 0.450 (Case C), and 0.632 (Case E), in the ranges $0.420 < X/L < 0.576$, $0.300 < X/L < 0.615$, and $0.302 < X/L < 0.616$, respectively. It is pertinent to mention that the velocity profiles near the drop wall and near the end of the recirculation zone are not included in determining the similarity profile. Because, the velocity profiles near the drop wall are influenced by the obstruction from the wall. On the other hand, at the end of the recirculation zone the bifurcation of the sliding jet affects the velocity profiles. Two similarity profiles are obtained for the variation of U_p in the recirculation zone using two characteristic length scales b and b_0. Initially, $-U_m$ and b_0 are considered as the characteristic velocity and length scales for attaining the similarity profile.

Figure 14(a) shows the similarity profile between dimensionless velocity $-U_p/U_m$ with dimensionless distance Y/b_0. It is pertinent to note that the $-U_p/U_m = 1$ occurs at nearly $Y/b_0 \approx 0.05$–0.1. After $Y/b_0 > 0.1$, U_p decreases and reaches zero at $Y/b_0 = 1$. However, another similarity profile is obtained by taking $-U_m$ and b as the characteristic velocity and characteristic length scales as plotted in Fig. 14(b). It is appealing to observe that both the similarity profiles have same degree of acceptance. Except that the similarity profile with length scale b_0 [Fig. 14(a)] has the data scatter for $Y/b_0 < 0.8$ and the similarity profile with length scale b [Fig. 14(b)] has the data scatter for $Y/b > 1.5$. However, the flow phenomena in the recirculation zone is similar to that of wall jets, hence, it is considered more suitable to use $-U_m$ and b as the appropriate characteristic scales in defining the mean velocity profile in the recirculation zone. Correspondingly, the regression equation given in Eq. (6) is obtained having R^2 value of 0.988. In Eq. (6), *erf*( ) represents the error function. The regression curve fits very well with the experimental data as illustrated in Fig. 14(b).

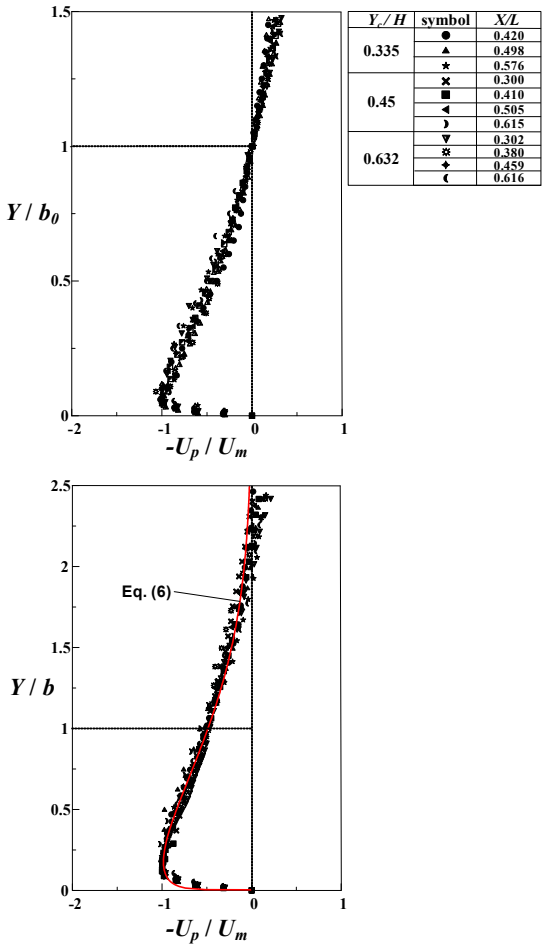


Fig. 14 Similarity profile for mean horizontal velocity in the recirculation zone: (a) $-U_p/U_m$ versus Y/b_0 and (b) $-U_p/U_m$ versus Y/b

$$-\frac{U_p}{U_m} = 1.49\left(\frac{Y}{b}\right)^{0.153}\left\{1 - erf\left[0.695\left(\frac{Y}{b}\right)\right]\right\} \qquad (6)$$

Further, the comparison between the similarity profiles for the mean horizontal velocity U_p in the recirculation zone obtained in the present study (for the skimming flow over vertical drop without end-sill) with those of skimming flow over vertical drop with end-sill and without ventilation (Lin, [23]) and of napped flow without end-sill and with ventilation (Lin *et al*., [8]) is shown in Fig. 16.

It is surprising to note that the similarity profiles for all the three cases follow the similar trend in the deflected jet portion near the bottom of the recirculation zone ($Y/b = 1$) irrespective of the ventilated condition and the end-sill effect. However, the position of maximum value of $-U_p/U_m$ is higher for the case of skimming flow with end-sill than the other two cases without end-sill. This is due to the cushioning effect imparted by the pool due to the presence of end-sill. On the other hand, for $Y/b > 1$ the profiles of skimming flow (present study and Lin, [23]) are similar. In contrast, for napped flow without end-sill and with ventilation (Lin *et al*., [8]) the profile deviates from the other

https://doi.org/10.1017/jmech.2012.115 Published online by Cambridge University Press

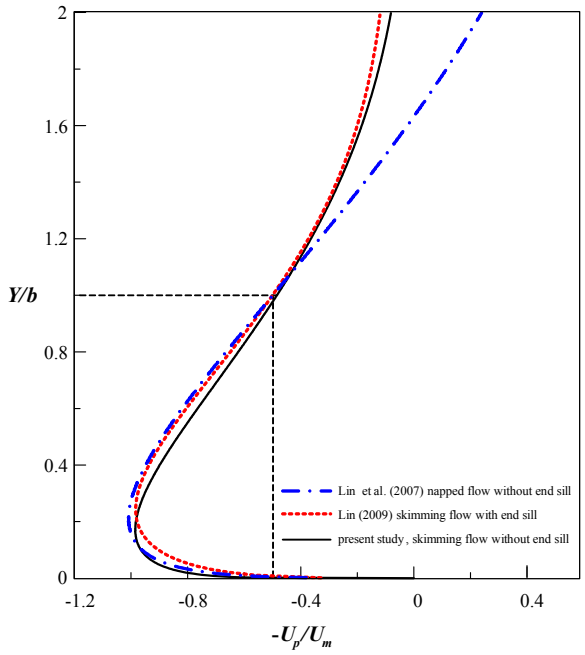


Fig. 15 Comparison of similarity profiles for mean horizontal velocity in recirculation zone of skimming flow and napped flow with and without end-sill

two curves of skimming flow for $Y/b > 1$ because Lin *et al*. [8] used b_0 as the length scale for similarity profile. In addition, the recirculation zone was in chaotic condition for napped flow. However, it is pertinent to note that, both the length scales b and b_0 are equally acceptable.

6. TURBULENCE CHARACTERISTICS IN SHEAR LAYER BETWEEN SLIDING JET AND RECIRCULATION ZONE

The turbulence characteristics including detailed distributions of velocity fluctuations, turbulence kinetic energy, viscous and Reynolds shear stresses, and turbulence energy budget balance in the shear layer between the sliding jet and recirculation zone are presented in this section. The mean streamwise velocity $U_s(Y_n)$ shown in Fig. 16(a) is used to demonstrate the experimental case of $Y_c/H = 0.450$ (Case C). However, the characteristics of $U_s(Y_n)$ are similar to that of other experimental cases of Y_c/H discussed earlier. Figure 16(b) illustrates the profiles of mean normal velocity $V_n(Y_n)$ in the shear layer between the sliding jet and the recirculation zone for case $Y_c / H = 0.450$ (Case C) at corresponding cross-sections as those of $U_s(Y_n)$. The mean normal velocity $V_n(Y_n)$ in the shear layer increases from the lower part of the shear layer in the upward direction attaining a maximum value and then decreases towards the free surface. The maximum value of $V_n(Y_n)$ is approximately about 15% – 20% of the maximum value of mean streamwise velocity $U_s(Y_n)$. Note that the maximum value of $V_n(Y_n)$ decreases in the downstream direction with increase in the arc-length position, S. This decreasing tendency of $V_n(Y_n)$ for S varying from 4.00cm to 8.98cm supports the larger momentum exchange near the drop wall and its reduction in the downstream direction. Nearly in the middle part of the sliding jet for 8.5cm < S < 9.5cm , the $V_n(Y_n)$ becomes relatively ill defined (not shown). However, the mean normal velocity $V_n(Y_n)$ has very prominent downward motion for Y_n ranging −3.0cm to −1.0cm in the most downstream part of the sliding jet (*e.g.*, S > 10.09cm). According to the observation of flow field during flow visualization tests, downward motion of the $V_n(Y_n)$ was evidenced and could be attributable to the local effect of very curving free surface over the most downstream part of the sliding jet.

The instantaneous velocity fields measured by HSPIV are used to attain the statistics of the fluctuating velocity field in the shear layer. Figure 16(c) represents the distributions of dimensionless turbulence intensities $(\overline{u'u'})^{0.5}/U_c$ and $(\overline{v'v'})^{0.5}/U_c$, and dimensionless kinetic energy $0.5(\overline{u'u'}+\overline{v'v'})/U_c^2$ for the experimental case $Y_c / H = 0.450$ (Case C) at respective cross-sections. Note that u' is the horizontal velocity fluctuation in the X-direction and v' is the vertical velocity fluctuation in the Y-direction. It is interesting to observe that profiles of both $(\overline{u'u'})^{0.5}/U_c$ and $(\overline{v'v'})^{0.5}/U_c$ follow the same trend in the entire shear layer region. The magnitudes of $(\overline{u'u'})^{0.5}/U_c$ and $(\overline{v'v'})^{0.5}/U_c$ are nearly equal in the regions above and below the shear layer, while in the shear layer structure, $(\overline{u'u'})^{0.5}/U_c$ slightly dominates over $(\overline{v'v'})^{0.5}/U_c$ at the beginning of the shear layer near the drop wall. However, $(\overline{v'v'})^{0.5}/U_c$ increases rapidly with the increase in arc length S and becomes greater than $(\overline{u'u'})^{0.5}$ for most part of the shear layer, say 6.05cm < S < 13.95cm. The profile of dimensionless turbulence kinetic energy, $0.5(\overline{u'u'}+\overline{v'v'})/U_c^2$ [see curves represented by red color in Fig. 16(c)], shows greater magnitude in the shear layer region than those in the regions above and below the shear layer. This trend is similar to the profiles of $(\overline{u'u'})^{0.5}/U_c$ and $(\overline{v'v'})^{0.5}/U_c$. On the other hand, the maximum value of $0.5(\overline{u'u'}+\overline{v'v'})/U_c^2$ is highest near the drop structure, which decreases gradually with an increase in arc length S. In addition, the variations of all the three parameters $(\overline{u'u'})^{0.5}/U_c$, $(\overline{v'v'})^{0.5}/U_c$ and $0.5(\overline{u'u'}+\overline{v'v'})/U_c^2$ exhibit bulge near the center position of the shear layer indicating larger magnitude of fluctuations, which gradually subsides towards the downstream. It should be noted that the flow in the shear layer is considered two-dimensional, therefore, the fluctuations in the spanwise (Z) direction, w' are not considered in computing turbulence kinetic energy as they are of relatively negligible magnitude.

Figure 16(d) represents the comparison of profiles of viscous shear stress and Reynolds shear stress along the shear layer at different arc-length positions of S for the

https://doi.org/10.1017/jmech.2012.115 Published online by Cambridge University Press

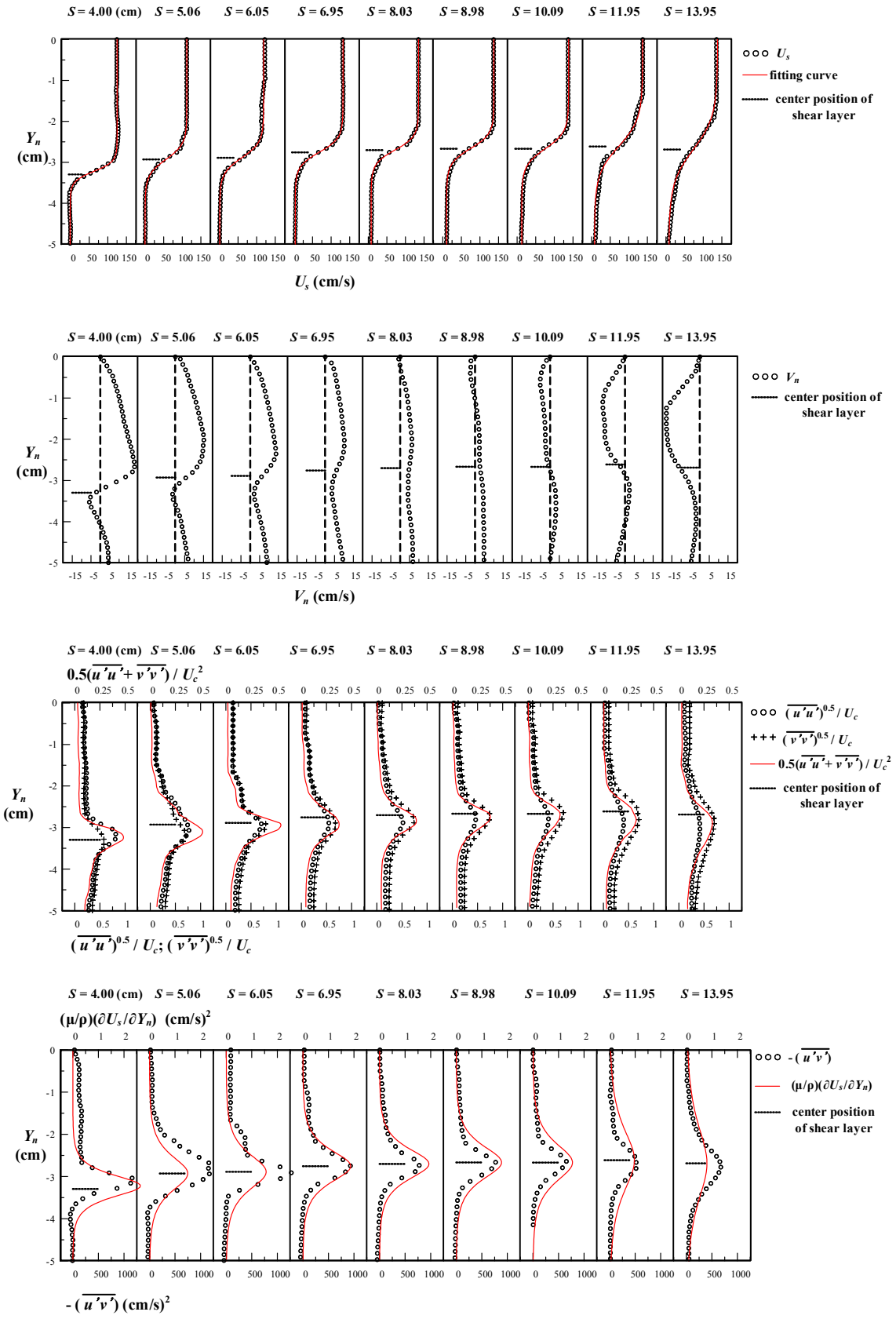


Fig. 16 Mean streamwise velocity profile $U_s(Y_n)$; (b) Mean normal velocity profile $V_n(Y_n)$; (c) $(\overline{u'u'})^{0.5}/U_c$, $(\overline{v'v'})^{0.5}/U_c$, and $0.5(\overline{u'u'}+\overline{v'v'})^{0.5}/U_c$; and (d) Reynolds shear stress $-(\overline{u'v'})$ and viscous shear stress $(\mu/\rho)(\partial U_s/\partial Y_n)$ for Case C ($Y_c/H = 0.450$)

https://doi.org/10.1017/jmech.2012.115 Published online by Cambridge University Press

experimental case Y_c / H = 0.450 (Case C). The viscous shear stresses $(\mu/\rho)(\partial U_s / \partial Y_n)$ are determined by differentiating the fitting curves of mean streamwise velocity $U_s(Y_n)$ with respect to Y_n, where μ is the dynamic viscosity of water and ρ is the mass density of water. On the other hand, the Reynolds shear stresses are expressed relative to ρ as $-(\overline{u'v'})$. Both viscous shear stress and Reynolds shear stress profiles follow similar trend as that of fluctuating velocity components and kinetic energy [Fig. 16(c)]. As seen from the distributions shown in Fig. 16(d) at each arch-length position, the magnitudes of viscous shear stress and Reynolds shear stress both start from zero at the free surface, then increase inwards and reach the bulge zone with their maximums right at the center of the shear layer Y_{nc}, and finally decrease to zero more inwards for $Y_n < -4.5$cm. Note that the maximum value of Reynolds shear stress is larger with an order of $O(10^2)$ than that of viscous shear stress. The Reynolds shear stress has highest value near the early part of shear layer, which tends to decrease towards the later part of the shear layer. From Fig. 16(d), it can be concluded that the Reynolds shear stresses dominate over viscous shear stresses for the entire length of shear layer. On an average, the maximum value of Reynolds shear stress is about 700 times the counterpart of viscous shear stress. This substantiates the dominance of momentum exchange as well as mixing process between sliding jet and recirculation zone in turbulent energy dissipation over the viscous friction.

7. TURBULENCE ENERGY BUDGET BALANCE IN SHEAR LAYER

According to Hinze [26], the turbulence energy-budget balance can be written as follows:

$$\underbrace{\frac{D\bar{k}}{Dt}}_{\text{(I)}} = \underbrace{-\frac{\partial}{\partial x_i}\overline{u_i'\left(\frac{p'}{\rho}+k\right)}}_{\text{(II)}} \underbrace{-\overline{u_i'u_j'}\frac{\partial U_j}{\partial x_i}}_{\text{(III)}} \underbrace{+\nu\frac{\partial}{\partial x_i}\overline{u'_j\left(\frac{\partial u_i'}{\partial x_j}+\frac{\partial u_j'}{\partial x_i}\right)}}_{\text{(IV)}} \underbrace{-\nu\overline{\left(\frac{\partial u_i'}{\partial x_j}+\frac{\partial u_j'}{\partial x_i}\right)\frac{\partial u_j'}{\partial x_i}}}_{\text{(V)}} \tag{7}$$

where k is the turbulent kinetic energy, U_j denotes the mean flow velocity in the jth component, and represent the velocity fluctuations in the ith and jth components, p' is the pressure fluctuation, is the kinematic viscosity of fluid, and x_i and x_j are Cartesian coordinates in the ith and jth directions. The (I) term in Eq. (7) shows the total change in turbulent kinetic energy per unit of mass and of time. Due to the steady flow condition in the present study, the first term depicting the local change in the turbulent kinetic energy, $k = (u'^2 + v'^2)/2$, can be neglected and the remaining terms expressed in the following are defined as the turbulence advection, T_A.

$$\frac{Dk}{Dt} = \cancel{\frac{\partial k}{\partial t}} + U_i\frac{\partial \bar{k}}{\partial x_i} = U\frac{\partial}{\partial x}\left[\frac{\overline{u'^2+v'^2}}{2}\right] + V\frac{\partial}{\partial y}\left[\frac{\overline{u'^2+v'^2}}{2}\right] = T_A \tag{8}$$

The (II) term in Eq. (7) depicts the work done by total dynamic pressure of turbulence which can be separated into two parts expressed by $-P_D$ and $-T_D$ and below:

$$-\frac{\partial}{\partial x_i}\left[\overline{u_i'\left(\frac{p'}{\rho}+k\right)}\right] = -\frac{\partial}{\partial x_i}\left(\frac{\overline{u_i'\,p'}}{\rho}\right) - \frac{\partial}{\partial x_i}(\overline{u_i'\,k}) = -P_D - T_D \tag{9}$$

$$P_D = \frac{\partial}{\partial x_i}\left(\frac{\overline{u_i'\,p'}}{\rho}\right) = \frac{\partial}{\partial x}\left(\frac{\overline{u'p'}}{\rho}\right) + \frac{\partial}{\partial y}\left(\frac{\overline{v'p'}}{\rho}\right) \tag{10}$$

$$T_D = \frac{\partial}{\partial x_i}(\overline{u_i'\,k}) = \frac{\partial}{\partial x}\frac{\overline{u'\cdot(u'^2+v'^2)}}{2} + \frac{\partial}{\partial y}\frac{\overline{v'\cdot(u'^2+v'^2)}}{2} \tag{11}$$

in which P_D denotes the pressure diffusion and T_D represents the turbulence diffusion. The (III) term in Eq. **(7)** illustrates the work of deformation of the mean motion by the turbulence stresses, which is well known as the turbulence production being denoted by T_P in the following:

$$-\overline{u_i'u_j'}\frac{\partial U_j}{\partial x_i} = -\overline{u'v'}\left(\frac{\partial U}{\partial y}+\frac{\partial V}{\partial x}\right) - \overline{u'^2}\frac{\partial U}{\partial x} - \overline{v'^2}\frac{\partial V}{\partial y} = T_P \tag{12}$$

Note that the (IV) term in Eq. (7) can be interpreted as the work by the viscous shear stresses of the turbulent motion and expressed below:

$$\begin{aligned}&\nu\frac{\partial}{\partial x_i}\overline{u'_j\left(\frac{\partial u_i'}{\partial x_j}+\frac{\partial u_j'}{\partial x_i}\right)}\\ &=\left(\frac{\mu}{\rho}\right)\left\{\frac{\partial}{\partial x}\overline{\left(\frac{\partial u'^2}{\partial x}\right)}+\frac{\partial}{\partial y}\overline{\left(\frac{\partial v'^2}{\partial y}\right)}+\frac{\partial}{\partial x}\overline{v'\left(\frac{\partial u'}{\partial y}+\frac{\partial v'}{\partial x}\right)}\right.\\ &\left.+\frac{\partial}{\partial y}\overline{u'\left(\frac{\partial u'}{\partial y}+\frac{\partial v'}{\partial x}\right)}\right\} = -V_D\end{aligned} \tag{13}$$

where V_D denotes the viscous diffusion. Finally, the (V) term in Eq. (7) shows the negative viscous dissipation by the turbulent motion and can be written as:

$$\begin{aligned}&-\nu\overline{\left(\frac{\partial u_i'}{\partial x_j}+\frac{\partial u_j'}{\partial x_i}\right)\frac{\partial u_j'}{\partial x_i}}\\ &=-\left(\frac{\mu}{\rho}\right)\left\{2\cdot\left[\overline{\left(\frac{\partial u'}{\partial x}\right)^2}+\overline{\left(\frac{\partial v'}{\partial y}\right)^2}\right]+\overline{\left(\frac{\partial u'}{\partial y}+\frac{\partial v'}{\partial x}\right)\cdot\frac{\partial v'}{\partial x}}\right.\\ &\left.+\overline{\left(\frac{\partial u'}{\partial y}+\frac{\partial v'}{\partial x}\right)\cdot\frac{\partial u'}{\partial y}}\right\} = -\varepsilon\end{aligned} \tag{14}$$

https://doi.org/10.1017/jmech.2012.115 Published online by Cambridge University Press

in which ε denotes the viscous dissipation. Based on the above-mentioned five terms of the turbulence energy-budget balance, the equation can be rewritten for brevity as

$$T_P = T_A + P_D + T_D + V_D + \varepsilon \tag{15}$$

At first, each distribution of six turbulence energy-budget terms, including turbulence production (T_P), turbulence advection (T_A), pressure diffusion (P_D), turbulence diffusion (T_D), viscous diffusion (V_D) and turbulence dissipation (ε) in the shear layer between sliding jet and recirculation zone at the arc-length position of $S = 4.0$ cm for $Y_c / H = 0.450$ (Case C) is presented in Fig. 17.

It can be realized from Fig. 17 that, near the drop structure (for S = 4.0cm), the turbulent production T_P has a relatively small negative value in the lower edge of the shear layer for $-2.5 < (Y_n - Y_{nc})/b_s < -1.5$, *e.g.*, $T_p = -18{,}570\text{cm}^2/\text{s}^3$ for $(Y_n - Y_{nc})/b_s = -1.87$. However, in the central part of shear layer, the value of turbulent production T_p increases greatly in magnitude (but with negative sign) for $-1.5 < (Y_n - Y_{nc})/b_s < 0$ and up to a negative maximum value of about $-220{,}000\text{cm}^2/\text{s}^3$ at the center of shear layer; and then decreases evidently in magnitude (also with negative sign) for $0 < (Y_n - Y_{nc})/b_s < 2.5$ and down to a small value for $(Y_n - Y_{nc})/b_s = 2.5$. Further, in the upper edge of shear layer for $(Y_n - Y_{nc})/b_s \geq 2.5$ the value of turbulence production T_p also has a relatively small value. Note that the viscous diffusion term V_D only has an insignificant **va**lue throughout the whole shear layer, *e.g.*, $V_D = -110\text{cm}^2/\text{s}^3$ being equivalent to 1/2000 times that of T_p at the center of shear layer, *i.e.*, $(Y_n - Y_{nc})/b_s = 0$. As regards the distributions of three remaining terms for the turbulence advection T_A, turbulence diffusion T_D and viscous dissipation ε in the central part of shear layer [for $-1.5 < (Y_n - Y_{nc})/b_s < 2.5$], all of their trends are similar to that of turbulence production T_p but with negative and positive signs for T_A, and T_D and ε, respectively. It is interesting to mention that, right at the center of shear layer, the negative maximum value of T_A is approximately $-14{,}000\text{cm}^2/\text{s}^3$ and the (positive) maximum values of T_D and ε are about $+55{,}000\text{cm}^2/\text{s}^3$ and $+2{,}500\text{cm}^2/\text{s}^3$, clearly justifying the ratios of T_A / T_P, T_D / T_P *and* ε / T_P being equal to about 1/15.7, and −1/4 and −1/88, respectively. Finally, the last remaining term, pressure diffusion P_D [shown in Eq. (10)], which can not be measured in the present study is thus calculated directly from the turbulence energy-budget balance equation, Eq. (15). It is found that from Fig. 17 the distribution of pressure diffusion P_D also has a very similar trend to that of the turbulence production in the central part of the shear layer, having the negative maximum value of about $-265{,}000\text{cm}^2/\text{s}^3$ (*i.e.*, $P_D = 1.2T_P < 0$) at the center of shear layer.

It is very interesting to note that near the drop structure (for smaller S) why the turbulence production T_P and thus pressure diffusion P_D have so large negative maximum values. As witnessed in Fig 3(b) and the corresponding close-up view of the velocity field near

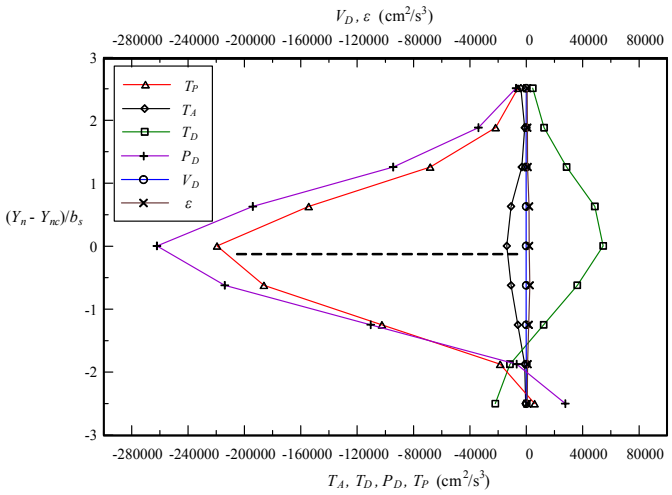


Fig. 17 Turbulence energy-budget balance in shear layer at $S = 4.0$ cm for Case C ($Y_c / H = 0.450$)

the drop structure shown in Fig. 3(c) for Case E as the supporting evidence, there does exist a prominent inclined upward flow toward the sliding jet, which is stemmed from the recirculation zone and entrained into the sliding jet. This inclined upward flow results in the transport of chaotic turbulence energy from the recirculation zone into the sliding jet. Therefore, the negative value of turbulence production T_p does reflect the energy exchange involving a loss to the chaotic recirculation zone and a supply to the (mean) sliding-jet flow. According to the detailed calculation of the three sub-terms for turbulence production T_P shown in Eq. (12), the second sub-term $(-\overline{u'^2}\cdot(\partial U/\partial x))$ can be defined as the work done by the kinetic energy of the horizontal velocity fluctuation transported by normal strain and has a negative maximum value about $-356{,}000\text{cm}^2/\text{s}^3$ right at the center of shear layer. On the other hand, the first and third sub-terms $\left(-\overline{u'v'}\cdot\left[(\partial U/\partial y)+(\partial V/\partial x)\right]\right.$ and $\left.-\overline{v'^2}\cdot(\partial V/\partial y)\right)$, which can be identified as the work done by the Reynolds shear stress carried by total shear strain and the work done by the kinetic energy of the vertical velocity fluctuation transported by normal strain, with the values of about $+90{,}800\text{cm}^2/\text{s}^3$ and $+45{,}600\text{cm}^2/\text{s}^3$, respectively, at the center of shear layer. The values of these three sub-terms in fact highlight the key negative contribution of turbulence production T_p is mainly from the second sub-term $(-\overline{u'^2}\cdot(\partial U/\partial x))$, because $(\overline{u'u'})$ is approximately equal to $(\overline{v'v'})$ (>> 0) as witnessed in Fig. 16(c) and the sliding jet of the skimming flow near the vertical drop structure accelerates downstream thus leading to $\partial U/\partial X > 0$ and $\partial V/\partial Y < 0$, with the magnitude of $|\partial V/\partial Y|$ is smaller than that of $\partial U/\partial X$.

Up to now, it is thus very clear that, near the drop structure, both viscous diffusion V_D as well as viscous dissipation ε nearly play no significant role and turbulence advection T_A has very minor role in turbulence energy-budget balance in the central part of shear layer.

https://doi.org/10.1017/jmech.2012.115 Published online by Cambridge University Press

In stead, turbulence production T_P, pressure diffusion P_D and turbulence diffusion T_D are the most important factors for balancing the turbulence energy budget.

Furthermore, all the six turbulence energy-budget terms, namely turbulence production (T_P), turbulence advection (T_A), pressure diffusion (P_D), turbulence diffusion (T_D), viscous diffusion (V_D) and turbulence dissipation (ε) along the shear layer between sliding jet and recirculation zone at different arc-length positions from S = 5.06cm to S = 13.95cm for the same Case C (Y_c / H = 0.450) are presented in Figs. 18(a) ~ 18(h). Note that throughout Figs. 18(a) ~ 18(h) the turbulence advection (T_A), turbulence diffusion (T_D), viscous diffusion (V_D) and turbulence dissipation (ε) are all very small, at most with O(10^{-1} ~ 10^{-3}) of the negative maximum value of T_P near the dropping structure. Their corresponding contributions in the turbulence energy-budget balance are not dominant and can be thus neglected without further discussion.

Combining Fig. 17 with Figs. 18(a) ~ 18(c) for S = 4.0cm ~ 6.95cm, the negative maximum values of turbulence production and pressure diffusion in the central part of shear layer are found to decrease considerably in magnitude with increase of the arc-length position *S, e.g.*, T_p = –220,000cm^2/s^3, –87,800cm^2/s^3, –23,000cm^2/s^3, –4,800cm^2/s^3 at S = 4.0cm, 5.06cm, 6.05cm, and 6.95cm, respectively. The reason for the turbulence production T_p having negative values for S = 5.06cm ~ 6.95cm is the same as that elucidated at S = 4.0cm (Fig. 17). Great care can be also taken to see each contribution of the above-mentioned three sub- terms to the turbulence production T_p [*i.e.*, Eq. (12)] at the arc-length position of S = 6.96cm where all of the six turbulence energy-budget terms have smaller values. For example, at $(Y_n - Y_{nc})/b_s$ = –0.16, the contribution of each sub-term [from the first to third term in the right-hand side of Eq. (12)] give the values of about +3,500cm^2/s^3, –83,500cm^2/s^3, and +78,100cm^2/s^3, respectively, thus leading to the turbulence production T_P with a small value of about –1,900cm^2/s^3 based on approximation by the order of magnitude. Note that the second and third sub-terms ($-\overline{u'^2}\cdot(\partial U/\partial x)$ and $-\overline{v'^2}\cdot(\partial V/\partial y)$) play major roles in the turbulence production than that of the first sub-term ($-\overline{u'v'}\cdot\left[(\partial U/\partial y)+(\partial V/\partial x)\right]$), but counteract to each other. The similar situation in each contribution of these three sub-terms is still hold throughout the whole shear layer for $-3.0 < (Y_n - Y_{nc})/b_s < 3.0$ for S = 6.95cm, demonstrating the energy exchange involving a very tiny loss to the chaotic recirculation zone and a very small profit to the (mean) sliding jet. On the contrary, it can

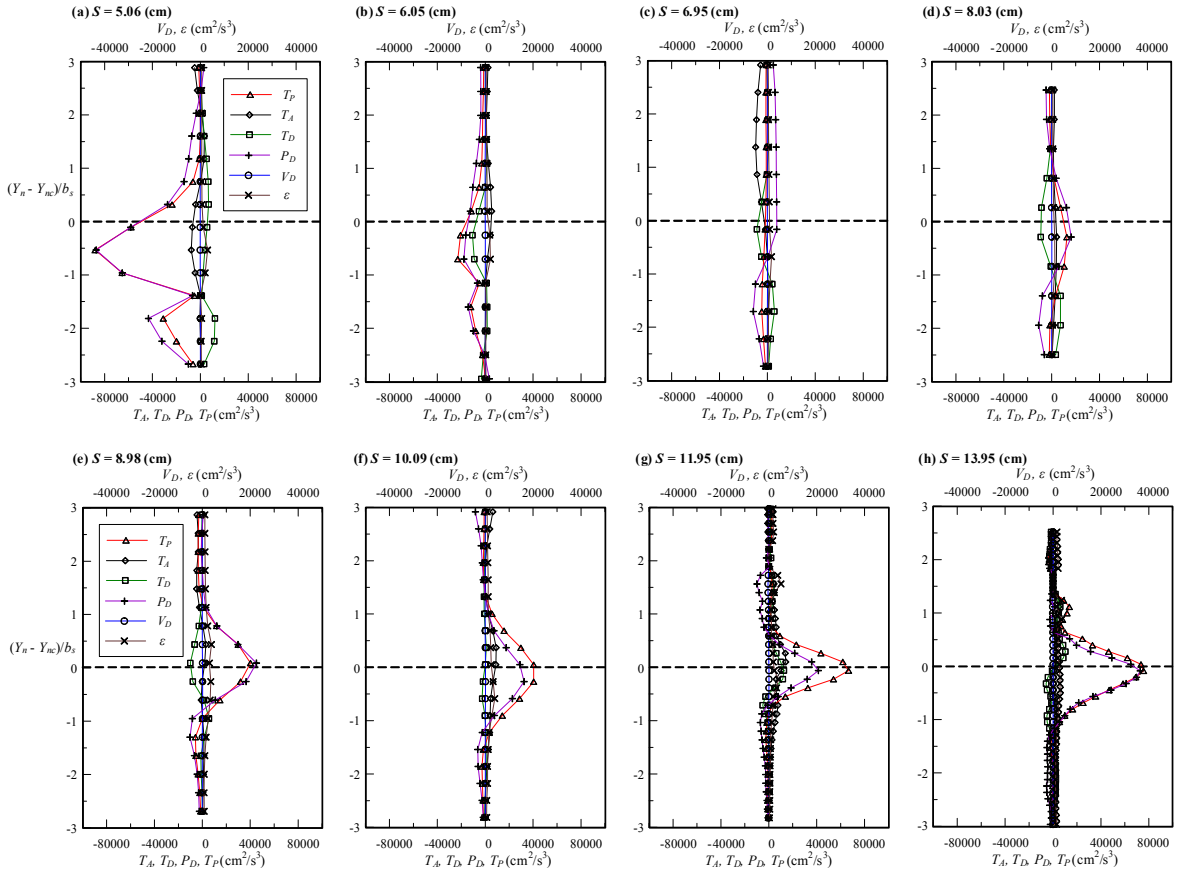


Fig. 18 Turbulence energy-budget balances in shear layer at different arc-length positions for Case C (Y_c /H = 0.450): (a) S = 5.06cm; (b) S = 6.05cm; (c) S = 6.95cm; (d) S = 8.03cm; (e) S = 8.98cm; (f) S = 10.09cm; (g) S = 11.95cm; and (h) S = 13.95cm

https://doi.org/10.1017/jmech.2012.115 Published online by Cambridge University Press

be seen from Fig. 18(d) that, at the arc-length position of S = 8.03cm, the turbulence energy-budget balance really shows a small supply to the chaotic recirculation zone and a small loss to the (mean) sliding jet because the values of turbulence production T_p are positive in the central part of shear layer for $-1.75 < (Y_n - Y_{nc})/b_s < 1.25$. The maximum value of T_P being equal to 12,700 cm^2/s^3 occurs at $(Y_n - Y_{nc})/b_s = -0.29$, where the values of turbulence advection T_A, turbulence diffusion T_D, viscous diffusion V_D, and viscous dissipation ε are +4200cm^2/s^3, –9,100cm^2/s^3, +20cm^2/s^3, and +1300cm^2/s^3, respectively, thus giving the value of pressure diffusion P_D being equal to 16,280cm^2/s^3 based on Eq. (15).

Further, it is found from Figs. 18(d) ~ 18(h) for S = 8.03cm ~ 13.95cm that the (positive) maximum values of turbulence production and pressure diffusion in the central part of shear layer increase with increase of the arc-length position S, *e.g.*, T_p = +12,800cm^2/s^3, +40,200cm^2/s^3, +45,000cm^2/s^3, +66,600cm^2/s^3, and +75,700cm^2/s^3 near the center of shear layer at S = 8.03cm, 8.98cm, 10.09cm, 11.95cm, and 13.95cm, respectively. The reason for the turbulence production T_p having positive values for S = 8.03cm ~ 13.95cm can be attributable to the prominent inclined downward flow near the horizontal base of vertical drop structure, which is generated from the sliding jet and then entrained into the recirculation zone. As witnessed from the full velocity field depicted in Fig 3(b) and the corresponding close-up view of the velocity field near the base shown in Fig. 3(d) for Case E, there really exists an inclined downward flow bifurcated from the mean sliding jet, thus resulting in transport of mean flow energy from the sliding jet into the turbulent recirculation zone. Therefore, the positive value of turbulence production T_p not only elucidates the energy exchange involving a supply to the chaotic recirculation zone and a loss to the (mean) sliding jet; but also illustrates the fact that the greater the arch length S (ranging from 8.03cm to 13.95cm), the larger the (positive) turbulence production in the central part of shear layer.

Once again, special attention can be also paid to explore each contribution of the above-mentioned three sub-terms in the turbulence production T_p [*i.e.*, Eq. (12)]. At the arc-length position of S = 13.95cm, the four turbulence energy-budget terms including T_A, T_D, and V_D and ε all have relatively small values; however, T_P and P_D both having nearly same positive values of about 75,700cm^2/s^3 near the center of shear layer. For example, at $(Y_n - Y_{nc})/b_s = -0.08$, the contribution of each sub-term [from the first to third term in the right-hand side of Eq. (12)] gives the value of about +600cm^2/s^3, –45,400cm^2/s^3, and +120,500cm^2/s^3, respectively, thus leading to the turbulence production T_P with a large value of about +75,700cm^2/s^3. Note that the third and second sub-terms ($-\overline{v'^2}\cdot(\partial V/\partial y)$ and $-\overline{u'^2}\cdot(\partial U/\partial x)$) play significant roles in the turbulence production T_P but counteract to each other, and the third sub-term ($-\overline{v'^2}\cdot(\partial V/\partial y)$) actually dominates in the energy transfer process.

As evidenced from Fig. 17 and Figs. 18(a) ~ 18(h), the viscous diffusion (V_D) and viscous dissipation (ε) are negligible in the turbulence energy-budget balance for the entire length of shear layer, which is subjected to the high turbulence characteristics in the shear layer of skimming flow.

8. CONCLUSIONS

From the view point of comprehensive understanding the flow structure within the shear layer and recirculation zone of the skimming flow over a vertical drop without end-sill and without ventilation, the laboratory experiments were carried out using HSPIV and flow visualization method. The findings of the study are:

1. The mean streamwise velocity distributions after the drop depict the occurrence of maximum overshoot of 105.4cm/s, which is also the maximum velocity throughout the whole thickness of dropping flow. In addition, the mean streamwise velocity in the shear layer have high velocity gradient near the drop structure, which decreases as the jet slides down the recirculation zone, demonstrating the momentum exchange and energy dissipation. The amount of energy loss in the skimming flow at the drop structure without ventilation is found to be greater than that with ventilation by an average value of 50% for $Y_c / H \geq 0.2$. However, for $Y_c / H < 0.2$, the variation of the relative energy loss approaches that of the ventilation case.
2. The sliding jet after being impinged at the floor gets deviated into the recirculation zone and forms a deflected jet having the characteristics similar to that of traditional wall jet following the similar phenomenon as that of the napped flow over vertical drop structure [Lin *et al*. [8]].
3. Two distinctive similarity profiles were obtained, one for mean streamwise velocity $U_s(Y_n)$ in the shear layer between the sliding jet and the recirculation zone and another for the mean horizontal velocity U_p in the recirculation zone. The velocity measurements taken with HSPIV at different sections for different flow conditions of Y_c / H are used to obtain the similarity profiles. The similarity profile for mean streamwise velocity $U_s(Y_n)$ in the shear layer between the sliding jet and the recirculation zone has been obtained by considering mean velocity deficit $(U_u - U_d)$ and representative thickness of shear layer b_s as the appropriate characteristic velocity and length scales. It is similar to the one proposed by Lin *et al*. [20] for the shear layer in the napped flow without end-sill and with ventilation and Lin *et al*. [23] for the shear layer in the skimming flow without end-sill and with ventilation. Further, the similarity profiles also encompass the experimental data points from the studies of traditional backward-facing step flow and cavity shear flow indicating the generality of the similarity profiles along with appropriate selection of characteristic scales.

https://doi.org/10.1017/jmech.2012.115 Published online by Cambridge University Press

4. On the other hand, the similarity profile for mean horizontal velocity U_p in the recirculation zone is determined using $-U_m$ and b as the characteristic velocity and length scales. This similarity profiles obtained for the recirculation zone is comparable with those of Lin [23] for skimming flow with end-sill and without ventilation and of Lin *et al*. [8] for napped flow without end-sill and with ventilation. However, due to the cushioning effect imparted by the pool due to the presence of end-sill the position of maximum value of $-U_p / U_m$ is higher for the case of skimming flow with end-sill than the other two cases without end-sill.
5. The detailed investigation on turbulence characteristics in the shear layer along with turbulent energy-budget balance is presented. It is found that at the beginning near the drop wall, $(\overline{u'u'})^{0.5}/U_c$ dominates over $(\overline{v'v'})^{0.5}/U_c$, while near the downstream end of the shear layer $(\overline{v'v'})^{0.5}/U_c$ increases rapidly and becomes greater than $(\overline{u'u'})^{0.5}/U_c$. The magnitude of turbulent kinetic energy $0.5(\overline{u'u'}+\overline{v'v'})/U_c^2$ has a greater magnitude in the shear layer region than those in the regions above and below the shear layer. The maximum value of $0.5(\overline{u'u'}+\overline{v'v'})/U_c^2$ is highest at the arc length position of S = 6.05cm and then decreases gradually with the increase in arc length S.
6. The profiles of both viscous shear stress and Reynolds shear stress follow similar trend as that of fluctuating velocity components and kinetic energy. The Reynolds shear stress dominates over viscous shear stress for the entire length of shear layer, having the maximum value of about 700 times the counterpart of viscous shear stress.
7. In the early part of developing shear layer near the drop structure, the turbulence production T_p shows very large negative values in the central part of shear layer, reflecting the fact that energy exchange involving a loss to the chaotic recirculation zone and a profit to the (mean) sliding-jet flow, which is caused by the inclined upward flow into the sliding jet. However, in the later part of the shear layer, turbulence production T_p on the contrary having large positive values just demonstrates the energy transfer being associated with a supply to the chaotic recirculation zone and a loss to the (mean) sliding jet, which is induced by the prominent inclined downward flow bifurcated from the (mean) sliding jet and entrained into the recirculation zone.
8. The analysis of turbulence energy-budget balance indicates turbulence production T_P, pressure diffusion P_D and turbulence diffusion T_D play important roles and turbulence advection T_A only has very minor role in turbulence energy-budget balance for the central part of the shear layer. Due to high turbulence characteristics in the shear layer of skimming flow, the viscous diffusion (V_D) and viscous dissipation are negligible in the turbulence energy-budget balance for the entire length of shear layer.

It is important to note that the large amount of measurement data including velocity fields, turbulence characteristics and turbulence energy-budget balance presented in this study become useful new data bank and it could be of great use for further study particularly in numerical simulations.

ACKNOWLEDGEMENTS

The authors gratefully acknowledge the financial supports of this work by National Science Council (NSC), Taiwan, under Grant Nos. NSC 99-2221-E-005-117-MY3 and NSC 100-2119-M-005- 001; and by the Directorate General of Highway as well as National Freeway Bureau of the Ministry of Transportation and Communication (MOTC), Taiwan.

NOTATIONS

The following symbols are used in this paper:

b = distance from floor of recirculation zone where $U_p = -U_m / 2$ [L];
b_s = representative thickness of shear layer, $(Y_{nu} - Y_{nd})$ [L];
b_s^* = practical thickness of shear layer, $(Y_{nu}^* - Y_{nd}^*)$ [L];
b_0 = distance from floor of pool where $U_p = 0$, defining edge of deflected jet, [L];
C_1 □ C_2 = regression coefficients [−];
E_1 = energy at upstream of drop structure [L];
E_2 = energy at downstream of drop structure [L];
ΔE = $E_1 - E_2$ [L];
F_r = approaching flow Froude number [−];
H = drop height [L];
k = turbulent kinetic energy [L^2T^{-2}];
L = length of recirculation zone [L];
P_D = pressure diffusion [L^2T^{-3}];
p' = pressure fluctuations [$ML^{-1}T^{-2}$];
q = approaching flow discharge per unit width [L^2T^{-1}];
S = coordinate distance along upper surface of sliding jet, arc length position [L];
T_A = turbulence advection [L^2T^{-3}];
T_D = turbulence diffusion [L^2T^{-3}];
T_P = turbulence production [L^2T^{-3}];
u' = fluctuation in U along X-direction [LT^{-1}];
U_a = approaching flow velocity [LT^{-1}];
U_c = critical velocity [LT^{-1}];
U_d = mean streamwise velocity in shear layer at Y_{nd} [LT^{-1}];
U_m = negative maximum velocity of deflected jet in recirculation zone ($U_m < 0$) [LT^{-1}];
U_p = mean horizontal velocity in recirculation zone [LT^{-1}];
U_s = mean streamwise velocity in shear layer [LT^{-1}];
U_u = mean streamwise velocity in shear layer at Y_{nu} [LT^{-1}];
U_∞ = mean stream velocity beyond shear layer [LT^{-1}];
v' = fluctuation in V along Y-direction [LT^{-1}];
V_D = viscous diffusion [L^2T^{-3}];

https://doi.org/10.1017/jmech.2012.115 Published online by Cambridge University Press

V_n = mean normal velocity [LT^{-1}];
X = streamwise distance in Cartesian coordinate system [L];
Y = vertical distance in Cartesian coordinate system [L];
Y_a = approaching flow depth [L];
Y_c = critical depth [L];
Y_p = depth of recirculation zone [L];
Y_n = coordinate distance outward normal to free surface [L];
Y_{nc} = center of shear layer [L];
Y_{nd} = lower bound of shear layer [L];
Y_{nd}^* = lower bound of shear layer at $\partial U_s / \partial Y_n \neq 0$ [L];
Y_{nu} = upper bound of shear layer [L];
Y_{nu}^* = upper bound of shear layer at $U_s = 0.99\ U_\infty$ [L];
Z = transverse (spanwise) distance in Cartesian coordinate system [L];
μ = dynamic viscosity of water [$ML^{-1}T^{-1}$];
ρ = mass density of water [ML^{-3}]; and
ε = viscous dissipation [L^2T^{-3}].

REFERENCES

1. Rouse, H., "Discharge Characteristics of the Free Overfall," *Civil Engineering*, **6**, p. 257 (1936).
2. White, M. P., "Discussion on Energy Loss at the Base of a Free Overfall," *Transactions*, ASCE, **108**, pp. 1361–1364 (1943).
3. Moore, W. L., "Energy Loss at the Base of Free Overfall," *Transactions America Society Civil Engineering*, **108**, pp. 1343–1360 (1943).
4. Rand, W., "Flow Geometry at Straight Drop Spillways," *Proceedings America Society Civil Engineering*, **81**, pp. 1–13 (1955).
5. Rajaratnam, N. and Chamani, M. R., "Energy Loss at Drops," *Journal of Hydraulic Research IAHR*, **33**, pp. 373–384 (1995).
6. Chamani, M. R. and Beirami, M. K., "Flow Characteristics at Drops," *Journal of Hydraulic Engineering*, ASCE, **128**, pp. 788–791 (2002).
7. Tokyay, N. and Yildiz, D., "Characteristics of Free Overfall for Supercritical Flows," *Canadian Journal of Civil Engineering*, **34**, pp. 162–169 (2007).
8. Lin, C., Hwung, W. Y., Hsieh, S. C. and Chang, K. A., "Experimental Study on Mean Velocity Characteristics of Flow over Vertical Drop," *Journal of Hydraulic Research IAHR*, **45**, pp. 33–42 (2007).
9. Chanson, H., "Discussion on Energy Loss at Drop," *Journal of Hydraulic Research IAHR*, **34**, pp. 273–278 (1996).
10. Huang, H. S., "Hydraulic Characteristics of Free Overfall-Impacted Channel Flow over Sloping Bed," *Ph.D. Thesis, Dept. of Civil Engineering*, National Chung- Hsing University, Taiwan (2010).
11. Chen, J. Y., Yao, C. Y., Liao, Y. Y. and Huang, H. S., "Impact Force on Downstream Bed of Weir by Free Overfall Flow," *Journal of the Chinese Institute of Engineers*, **31**, pp. 1047–1055 (2008).
12. Chen, J. Y., Huang, H. S., Hong, Y. M. and Liu, S. I., "The Impact Characteristics Analysis of Free Overfall Flow on a Downstream Channel Bed," *Journal of the Chinese Institute of Engineers*, **34**, pp. 403–413 (2011).
13. Etheridge, D. W. and Kemp, P. H., "Measurements of Turbulent Flow Downstream of a Rear-Facing Step," *Journal of Fluid Mechanics*, **86**, pp. 545–566 (1978).
14. Armaly, B. F., Durst, F., Pereira, J. C. F. and Schonung, B., "Experimental and Theoretical Investigation of Backward-Facing Step Flow," *Journal of Fluid Mechanics*, **127**, pp. 473–496 (1983).
15. Troutt, T. R., Scheelke, B. and Norman, T. R., "Organized Structures in a Reattaching Separated Flow Field," *Journal of Fluid Mechanics*, **143**, pp. 413–427 (1984).
16. Grant, I., Owens, E. and Yan, Y. Y., "Particle Image Velocimetry Measurements of the Separated Flow Behind a Rearward Facing Step," *Experiments in Fluids*, **12**, pp. 238–244 (1992).
17. Pereira, J. C. F. and Sousa, J. M. M., "Experimental and Numerical Investigation of Flow Oscillations in a Rectangular Cavity," *Journal of Fluids Engineering, ASME Transaction*, **117**, pp. 68–74 (1995).
18. Kuo, C. H., Huang, S. H. and Chang, C. W., "Self-Sustained Oscillation Induced by Horizontal Cover Plate Above the Cavity," *Journal of Fluids and Structural*, **14**, pp. 25–48 (2000).
19. Kuo, C. H. and Jeng, W. I., "Lock-On Characteristics of a Cavity Shear Layer," *Journal of Fluids and Structural*, **18**, pp. 715–728 (2003).
20. Lin, C., Hwung, W. Y., Hsieh, S. C. and Chang, K. A., "Reply to the Discussion: Experimental Study on Mean Velocity Characteristics of Flow over Vertical Drop," *Journal of Hydraulic Research IAHR*, **46**, pp. 425–428 (2008a).
21. Kiyani, G. A. and Rajaratnam, N., "Discussion: Experimental Study on Mean Velocity Characteristics of Flow over Vertical Drop," *Journal of Hydraulic Research IAHR*, **46**(3), pp. 424–425 (2008).
22. Lin, C., Hsieh, S. C., Kuo, K. J. and Chang, K. A., "Periodic Oscillation Caused by a Uniform Flow over a Vertical Drop Energy Dissipator," *Journal of Hydraulic Engineering*, ASCE, **134**, pp. 948–960 (2008b).
23. Lin, W. J., "Flow Characteristics in Skimming Flow over a Vertical Drop Pool," Ph.D. Thesis, Department of Civil Engineering, National Chung Hsing University, Taiwan (2009).
24. Jaung, R. H., "Study on the Characteristics of Periodic Oscillation Downstream of Plunging Pool," Master Thesis, Department of Civil Engineering, National Chung Hsing University, Taiwan (2000).
25. Chou, S. H., "Study on the Characteristics of Skimming Flow," Master Thesis, Department of Civil Engineering, National Chung Hsing University, Taiwan (2008).
26. Hinze, J. O., *Turblence*, McGRAW-HILL, New York (1959).

(Manuscript received August 12, 2011, accepted for publication May 9, 2012.)

https://doi.org/10.1017/jmech.2012.115 Published online by Cambridge University Press